AECL

INTERNATIONAL STANDARD PROBLEM ISP-41 FU/1 PDF FOLLOW-UP EXERCISE (Phase 1):

Containment Iodine Computer Code Exercise: Parametric Studies

By

J. Ball[1] G. Glowa[1], J. Wren[1], F. Ewig[2], S.Dickenson[3], Y. Billarand[4], L. Cantrel[4], A. Rydl[5] and J. Royen[6]

ABSTRACT

This report describes the results of the second phase of International Standard Problem (ISP) 41, an iodine behaviour code comparison exercise. The first phase of the study, which was based on a simple Radioiodine Test Facility (RTF)experiment, demonstrated that all of the iodine behaviour codes had the capability to reproduce iodine behaviour for a narrow range of conditions (single temperature, no organic impurities, controlled pH steps). The current phase, a parametric study, was designed to evaluate the sensitivity of iodine behaviour codes to boundary conditions such as pH, dose rate, temperature and initial I^- concentration. The codes used in this exercise were IODE(IPSN), IODE(NRIR), IMPAIR(GRS), INSPECT(AEAT), IMOD(AECL) and LIRIC(AECL). The parametric study described in this report identified several areas of discrepancy between the various codes. In general, the codes agree regarding qualitative trends, but their predictions regarding the actual amount of volatile iodine varied considerably. The largest source of the discrepancies between code predictions appears to be their different approaches to modelling the formation and destruction of organic iodides. A recommendation arising from this exercise is that an additional code comparison exercise be performed on organic iodide formation, against data obtained from intermediate-scale studies (two RTF (AECL, Canada) and two CAIMAN facility (IPSN, France) experiments have been chosen). This comparison will allow each of the code users to realistically evaluate and improve the organic iodide behaviour sub-models within their codes.

Fuel Safety Branch
Chalk River Laboratories
Chalk River, Ontario K0J 1J0

---

[1]AECL (Canada)
[2]GRS Koln (Germany)
[3]AEAT (UK)
[4]IPSN (France)
[5]NRIR (Czech Republic)
[6]OECD/NEA

EXECUTIVE SUMMARY

As the nuclear industry attempts to increase the reliability and economic viability of nuclear plants, future safety analysis will rely even more on iodine behaviour codes. Attempts to reduce the exclusion boundary area, to extend the life of existing nuclear power plants, and to develop new safety concepts for advanced reactor designs have resulted in new requirements for safety analyses. There is increasing demand for the safety analyses of reactor accident consequences to move from bounding conservative estimates towards best estimates that are supported with uncertainty analyses. These changes require regulatory approval, and methodologies based on out-dated knowledge and bounding estimates are expected to be inadequate.

To meet current and future demands, it is necessary that iodine codes demonstrate their ability to provide accurate estimates of iodine volatility for a large range of reactor accident scenarios. Unfortunately, simple correlations between iodine volatility and key parameters (e.g., scaling, temperature, dose rate, pH, initial iodine speciation, organic impurities, surfaces, etc.) are not readily obtained from experimental data obtained under a narrow range of conditions. Furthermore, one cannot easily determine representative accident conditions. For an iodine behaviour code to be confidently applied to modelling accident conditions, it should therefore be able to reproduce experimental data obtained under a wide range of conditions.

The first ISP 41 comparison exercise was based on a simple Radioiodine Test Facility (RTF) experiment and demonstrated that all of the iodine behaviour codes had the capability to reproduce iodine behaviour for a narrow range of conditions (single temperature, no organic impurities, controlled pH steps). However, the exercise also demonstrated that the performance of these codes is extremely reliant upon the judicious choice of user-defined kinetic parameters. If code calculations are to be used as predictive or interpretive tools, then the kinetic parameters used in the codes must be applicable to the entire range of conditions that are anticipated in post-accident containment.

The second step of ISP 41 (the work reported in this document) was an opportunity for code users to assess their codes over a wide range of accident conditions. The exercise examined the sensitivity of code output to input parameters such as pH, dose rate, initial iodine concentration, and the presence of organic impurities, painted surfaces, and silver. The parametric study identified several areas of discrepancy between the various codes. In general, the codes agree regarding qualitative trends, but the actual amount of volatile iodine predicted by each of the codes varies considerably. The largest source of the discrepancies between code predictions appears to be the differences in modelling the formation and destruction of organic iodides in each code.

Ideally, the results of step 1 and step 2 of the ISP 41 exercise should be used to improve the organic iodide sub-models within the iodine behaviour codes. Although the exercise identified the organic iodide sub-model as one of the most significant contributors to the discrepancy

between the code predictions, the calculations cannot tell us which (if any) of the sub-models are correct, and what the range of user-defined input parameters for each of the sub-models could be. The next logical step of the ISP 41 exercise is the performance of code comparison exercises against experimental data on organic iodide formation, preferably data obtained over as large a range of experimental conditions as possible. This comparison will allow each of the code users to realistically evaluate and improve the organic iodide behaviour sub-models within their codes.

In the interest of covering as large a range of experimental conditions as possible, we recommend that the final step of ISP 41 be a code comparison against four intermediate scale studies: two Caiman facility experiments, and two RTF experiments, which were performed over a very large range of experimental conditions (dose rate, painted surface areas, temperature, pH, etc.). We recommend that the calculations be performed first as blind calculations (i.e., each code is used with default parameters). Subsequently, the results can be made available to each of the participants, and a second set of calculations can be performed, in which user-defined kinetic parameters (such as those within the organic iodide sub-models) are optimized to provide a best fit to all of the experimental data. In each of the experiments, the presence of painted surfaces resulted in organic iodides contributing significantly to the volatile iodine fraction. This comparison exercise should therefore provide insight into the performance of the organic iodide models in each code. The exercise will provide code users with improved values for the user-defined input parameters in their iodine behaviour codes. The exercise may also provide insight into the organic iodide formation and destruction mechanisms, and identify whether future experiments or changes in modelling strategy are required.

The main objective of ISP exercises is to increase confidence in the validity and accuracy of the tools that are used in assessing the safety of nuclear installations. The secondary objective is to enable code users to gain experience and demonstrate their competence. Due to the complexity of iodine behaviour in containment, the ISP 41 exercise on iodine codes has required three steps to achieve these objectives, which are

1. ISP 41: Computer code exercise based on a simple RTF experiment on iodine behaviour in containment under severe accident conditions.
2. ISP 41 Follow-up Step 1: Parametric calculations.
3. ISP 41 Follow-up Step 2: Computer code exercise based on complex experiments performed at the RTF and Caiman facilities.

We have completed the first two steps and recommend completing the final step.

1. INTRODUCTION

International Standard Problem (ISP) exercises are comparative exercises, in which predictions of different computer codes for a given physical problem are compared with each other, or with the results of a carefully controlled experimental study. The main goal of ISP exercises is to increase confidence in the validity and accuracy of the tools that are used to assess the safety of nuclear installations. Moreover, the exercises enable code users to gain experience and demonstrate their competence.

The ISP 41 exercise, a comparison of iodine behavior models, was first proposed at the Fourth Iodine Chemistry Workshop held at the Paul Scherrer Institute (PSI), Switzerland in 1996 June. The results of a Radioiodine Test Facility (RTF) experiment were made available by CANDU® Owners Group (COG) for the exercise. An RTF experiment performed under controlled and limited conditions was chosen as a starting point for the evaluation of the various iodine behavior codes, in the hope that the basic components of each code could be compared. The experiment was ideal for demonstrating the ability of all of the codes to model the influence of pH on iodine volatility, one of the most important aspects of iodine behaviour. Participants were given details of the experimental set-up, conditions and procedures of the RTF test, and they were asked to calculate experimentally observed parameters, such as the total concentration and speciation of iodine in the gas and aqueous phases, and the distribution of iodine at the end of the test between the gas phase, the aqueous phase and surfaces that were exposed to each of these phases.

Results from the first step of ISP 41 are detailed elsewhere [1]. The objective of the exercise, which was to evaluate the basic components of each code, and to demonstrate their ability to simulate experimental results under controlled conditions, was achieved. The exercise established that the pH dependence of iodine volatility can be accurately reproduced by all codes used in the study.

The following additional conclusions arose from the first step of ISP 41:

1. The performance of the iodine behavior codes is extremely reliant upon the judicious choice of user-defined kinetic parameters, many of which have been chosen to provide a best fit of the code output to experimental data obtained under a narrow range of conditions (such as temperature, dose rate, iodide concentrations, etc.).

2. In order to use code calculations as predictive or interpretive tools, it must be demonstrated that the kinetic parameters used in the codes are applicable to the entire range of conditions anticipated in post-accident containment.

These conclusions, and the recognition that the first step of the comparison exercise did not evaluate several aspects of code performance (e.g., the ability to predict pH, and organic iodide formation) led to the recommendation that two follow-up exercises be performed as part of ISP

---

41. The first phase of these follow-up exercises, consisting of a set of parametric studies, is described in this document.

The parametric studies described in this document were designed to evaluate the sensitivity of iodine behaviour codes to boundary conditions such as pH, dose rate, temperature and initial I^- concentration. The comparison of code results over a wide range of conditions is necessary to understand where the codes agree and where they diverge, so that a strategy for further code development, application and validation can be developed. The results of the parametric study will also determine the readiness of each code for the proposed second phase of the exercise, i.e., a blind code comparison test using two intermediate scale studies that are more complex than the RTF experiment used for the initial step of ISP 41.

The range of conditions for the parametric calculations are

pH	4 - 10
temperature	60 - 130 °C
dose rate	0.1 - 10 $kGy \cdot h^{-1}$
initial I^- concentration	10^{-6} - 10^{-4} $moles \cdot dm^{-3}$

The effect of steam condensation, the presence of Ag, and the availability of organic materials in the aqueous phase were also examined in the exercise. A full description of the parametric matrix can be found in Appendix A.

2. THE IODINE BEHAVIOUR CODES

The iodine behaviour codes used in this comparison exercise were IODE 4.2 (IPSN), LIRIC 3.2 (AECL), IMOD 2.0 (AECL), INSPECT (AEAT), IMPAIR (GRS) and modified IODE(NRIR). The purpose of each of these codes is to describe chemical and physical processes that influence iodine behaviour, under conditions that are relevant to post-accident containment. Therefore, the fundamental components of each of these codes are similar. Each code contains sub-models for key processes, such as

1. the interconversion between non-volatile iodine species (e.g., I^-, IO_3^-) and volatile iodine species (I_2) in the aqueous and gas phases,
2. the formation and destruction of organic iodides,
3. the transport of volatile species (e.g., I_2, RI) across a liquid-gas interface,
4. the transport of iodine species to (adsorption) and from (desorption) surfaces, and
5. the transport of iodine species to condensing films and to the bulk aqueous phase by condensation flows.

A brief description of the method by which the codes model each of these processes is provided below.

2.1 Interconversion Between Iodine Species

The iodine behaviour codes used in the current exercise model the hydrolysis of molecular iodine in essentially the same way [1, 2]:

$$I_2 + H_2O = HOI + I^- + H^+ \quad (1)$$

$$HOI = OI^- + H^+ \quad (2)$$

$$3HOI = IO_3^- + 2I^- + 3H^+ \quad (3)$$

Therefore, it is only in the radiolytic reaction subset that the interconversion of iodine species is modelled differently[1].

In LIRIC and INSPECT, a mechanistic model is used to calculate the concentrations of the water radiolysis species that subsequently react with various iodine and organic species to produce volatile iodine species, and reduce these volatile species back to non-volatile iodide. The key radiolytic reactions are

Primary water radiolysis

$$4.1\ H_2O \xrightarrow{h\nu} 2.6\ e_{aq}^- + 0.6\ \bullet H + 2.7\ \bullet OH + 0.7\ H_2O_2 + 2.6\ H^+ + 0.45\ H_2 \quad (4a)$$

[1] IMOD does not explicitly contain the I_2 hydrolysis reactions. However, IMOD was constructed from LIRIC; the overall rates for volatile iodine production and decomposition used in IMOD reflect the hydrolysis processes.

where the coefficients in Reaction (4a) are the G-values for the primary production from γ-radiolysis of water in units of molecules per 100 eV absorbed dose.

Secondary reactions of the primary water radiolysis products with each other and with organic and inorganic impurities (4b)

Oxidation and reduction of iodine species[2]

$$2I^- + 2{\bullet}OH \rightarrow I_2(aq) \quad (5)$$
$$I_2(aq) + 2O_2^- \rightarrow 2I^- + 2O_2 \quad (6)$$
$$I_2(aq) + H_2O_2 \rightarrow 2I^- + 2H^+ + O_2 \quad (7)$$

Reactions (5–7) in LIRIC and INSPECT are dependent upon the dose rate. Reactions (1–3) and (6) and (7) are extremely dependent upon the aqueous pH, and Reactions (1) and (7) have strong temperature dependences.

IODE and IMPAIR use two equations to model the radiolysis of iodine species in the aqueous phase. In IODE, the equations are

$$2I^- \xleftrightarrow{h\nu} I_2 \quad (8)$$
$$I_2 + 3\,O_2 \xleftrightarrow{h\nu} 2\,IO_3^- \quad (9a)$$

The pH and dose rate dependence of molecular iodine formation in IODE is incorporated into the rate equations in the following manner:

Rate of I_2 production by (8) $= d[I_2]/dt = k_8\,[I^-]\cdot[H^+]^n\cdot D - k_{-8}[I_2]$ (10)
Rate of I_2 production by (9a) $= d[I_2]/dt = k_{-9a}\,[IO_3^-]\cdot[H^+]^n\cdot D - k_{9a}[I_2]$ (11a)

where D is the dose rate in $Gy\cdot s^{-1}$, and n is a user-defined exponential term.

IMPAIR also contains Reaction (8) with a rate expression similar to that for IODE, but with different values for the rate constants and the exponent, and with D expressed in units of $kGy\cdot h^{-1}$. IMPAIR also contains the forward reaction of (9a); however, instead of I_2 being reversibly converted to IO_3^-, the iodine oxidation reaction is an irreversible process that is represented by

$$I_2 + 3\,O_2 \rightarrow 2\,IO_3^- \quad (9b)$$

with the following rate equation:

$$d[I_2]/dt = -k_9[I_2] \quad (11b)$$

[2] Note that Reactions (5) through (7) are written as overall reactions that consist of more than one step. The codes model the individual steps separately.

Iodate is then irreversibly converted to iodide:

$$2IO_3^- \xrightarrow{h\nu} I^- + 3O_2 \qquad (12)$$

with its rate defined as

$$d[IO_3^-] / dt = -k_{12}[IO_3^-]^n \cdot D \qquad (13)$$

IMOD uses Reaction (8) to represent the overall (both thermal and radiolytic) interconversion of iodine species in the aqueous phase, with the rate expression formulated to reproduce, as closely as possible, the overall pH, temperature and dose rate dependence of overall volatile iodine production predicted by LIRIC, over a wide range of conditions. That is, Reactions (1–7) and any iodate formation and reduction in LIRIC are represented by Reaction (8) in IMOD. In IMOD, the rate equation is further simplified such that the rate of production of volatile iodine species (i.e., the forward rate of Reaction (8)) is dependent only on dose rate and is independent of pH and temperature. In contrast, the backward rate (reduction of I_2 to I^-) is pH-, temperature- and dose-rate-dependent.

2.2 Organic Iodide Formation and Decomposition

The sub-models for the radiolysis of organic species and the formation and decomposition of organic iodides are treated quite differently in each of the various iodine behaviour codes. LIRIC and IMOD contain essentially the same sub-model to describe these processes. These codes, along with IODE(NRIR), assume that organic iodide formation is primarily an aqueous-phase process, initiated by the radiolytic decomposition of organic solvents in the aqueous phase (Reactions (14–16)). The decomposition of organic iodides by hydrolysis (Reaction (17)) and radiolysis (Reaction (18)) is also incorporated into these codes.

The model for organic iodide formation in LIRIC and IMOD is[3]

$$RH + {\bullet}OH \rightarrow R{\bullet} + H_2O \qquad (14)$$
$$R{\bullet} + O_2 \rightarrow RO_2{\bullet} \rightarrow\rightarrow CO_2 \qquad (15)$$
$$R{\bullet} + I_2/HOI \rightarrow RI + I{\bullet} \qquad (16)$$
$$RI + H_2O/OH^- \rightarrow I^- + H^+ + ROH \qquad (17)$$
$$RI + e^-_{aq} \rightarrow I^- + R{\bullet} \qquad (18)$$

[3] The organic sub-models in LIRIC and IMOD differ only in the way they calculate the OH concentration. In LIRIC, the OH concentration is modelled in detail using the full water radiolysis reaction set, whereas in IMOD, the OH concentration is expressed using a simple algebraic formula.

In these models, the formation of organic iodides is dose-rate-dependent, because the rate of production of both R• and I_2 are dependent upon the dose rate (•OH radical concentration affects both production rates). However, because RH and I^- compete with each other for •OH radicals, an increase in the dose rate by a given factor does not result in a linear increase in both the amount of I_2 and R•. The dose rate dependence of organic iodide formation in LIRIC and IMOD is not as strong as it is in some of the other codes, which assume that the formation of I_2 and the formation of organic iodides each have separate and additive dependences on the dose rate (see Reactions (22–27) below).

In LIRIC and IMOD, the concentration of the organic species RH(aq) is assumed to be dependent upon its rate of accumulation in the aqueous phase, as a result of dissolution from wetted or immersed painted surfaces (as well as being dependent upon its rate of depletion by Reaction (14)). The rate of accumulation is described as a temperature-dependent, first-order kinetic process:

$$[RH(aq)]_t = [RH(aq)]_\infty \cdot \left(1 - \exp\left(-k_{DIS} \cdot t\right)\right) \qquad (19)$$

where $[RH(aq)]_t$ and $[RH(aq)]_\infty$ represent the concentrations of organic compound in the aqueous phase at time t, and when dissolution is complete, respectively, and k_{DIS} is the dissolution rate constant (s^{-1}). $[RH(aq)]_\infty$ ($mol \cdot dm^{-3}$) is determined by the initial amount of solvent that is available in the paint polymer to be released into a given volume of water, and is a function of temperature, coating thickness and paint age. The rate constant k_{DIS} is also dependent upon these parameters.

IODE(NRIR) formulates organic iodide formation in the aqueous phase using a simple first-order equation (see Reaction (20) below), and does not incorporate an organic solvent accumulation process into the model; instead, it assumes an initial [RH](aq) that is independent of temperature, and is user-defined. For this exercise, IODE(NRIR) assumed an initial concentration of 1×10^{-3} $mol \cdot dm^{-3}$ for all calculations. In addition, the organic iodides are modelled in IODE(NRIR) to decompose only by hydrolysis, (Reaction (17)), and not by radiolysis (Reaction (18)).

In IODE(IPSN) and IMPAIR, organic iodide formation can occur both by aqueous-phase processes and heterogeneous processes:

a. Aqueous homogeneous thermal process

$$I_2(aq) + 2\ CH_3R(aq) \rightleftarrows 2\ CH_3I(aq) + 2\ R(aq) \qquad (20)$$

with the rate defined as

$$d[CH_3I(aq)]/dt = k_{20}\,[I_2(aq)]\,[CH_3R(aq)] - k_{-20}\,[CH_3I(aq)] \qquad (21)$$

b. Heterogeneous thermal and radiolytic process

$$\text{Paint} + I_2(s) \text{ or } I^-(s) \rightleftarrows CH_3I(g,aq) + R(s) \quad (22)$$

with the rate defined as

$$\text{in IMPAIR:} \quad d[CH_3I]/dt = (A/V_g)\,(k_{22} + k_{22}^{rad}\,D)\,[H^+]^{0.24}\,(2\,[I_2(s)] + [I^-(s)]) \quad (23a)$$

$$\text{in IODE(IPSN):} \quad d[CH_3I]/dt = (A/V_g)\,(k_{22} + k_{22}^{rad}\,D)\,[H^+]^{0.24}\,(2\,[I_2(aq)] + [I^-(aq)]) \quad (23b)$$

where A is the total (dry and submerged) paint surface area, V is the volume of the gas phase, and (s) refers to deposited species. In IMPAIR, the concentrations of deposited species ($I_2(s)$ and $I^-(s)$) are calculated by the iodine absorption sub-model. Note that although Reaction (22) in IODE(IPSN) is a surface process, the rate of production of CH_3I is formulated using the aqueous-phase concentrations of I_2 and I^-, rather than the surface concentrations. The implicit assumption is that the surface concentrations of the iodine species are proportional to the aqueous concentrations.

Organic iodide formation is very pH dependent as a result of the formulation of Equation (23). This direct pH dependence, resulting from the $[H^+]^{0.24}$ term, is augmented by the dependence of $I_2(aq)$ or $I_2(s)$ on pH. As a result, organic iodide formation in both of these codes is more strongly dependent on pH than it is in LIRIC and IMOD.

The dose rate dependence of organic iodide formation in IMPAIR is a function of the amount of iodine that is predicted to be deposited on surfaces. The overall rates of organic iodide formation via Reactions (20) and (22) are proportional to the dose rate, because the rate of production of I_2 is dose-rate-dependent. In addition, Reaction (22) has an extra dose rate dependence resulting from the $k_{22}^{rad}D$ term. However, if appreciable I^- is deposited on the surface, and if k_{22} is larger than k_{22}^{rad}, then there is a pathway to the formation of organic iodides that is independent of the dose rate.

The initial concentration of organic species, $[CH_3R]$, is a user-defined input in both IODE(IPSN) and IMPAIR. For this exercise, calculations using these codes assumed that the concentration was 0, with the exception of Case 8, where the amount of organic species was specified. Therefore, for all the other cases, both codes modelled organic iodide formation as a surface process alone.

The decomposition of CH_3I by hydrolysis, Reaction (17), is included in both IODE(IPSN) and IMPAIR. IMPAIR calculations assumed that there was radiolytic decomposition of organic iodides in both the gas and aqueous phases (Reaction 24), with k_{24} defined as 1.6×10^{-4} s^{-1}, and 3×10^{-4} s^{-1} respectively. However, although IODE(IPSN) contains the same radiolytic decomposition mechanism (but only in the aqueous phase), the calculations performed for this exercise did not use this decomposition process:

$$CH_3I(g,aq) + h\nu \longleftrightarrow I_2(g,aq) + 2\,CH_3\bullet\,(g, aq) \quad (24)$$

$$-d[CH_3I]/dt = k_{24}\, D\, [CH_3I] - k_{-24}\, [I_2]\, [CH_3\bullet] \quad (25)$$

INSPECT assumes that all of the organic iodides are produced by a surface process that is based on a model developed by Funke [2], which is similar to that in Reaction (22):

$$\text{Paint} + \text{DEP} \rightleftarrows CH_3I(g) + R\bullet \quad (26)$$

$$d[CH_3I(g)]/dt = (A/V_g)\,(k_{26} + k_{26}^{rad}\, D)[DEP] - k_{dec}[CH_3I(g)]D \quad (27)$$

where $[CH_3I(g)]$ = CH_3I concentration in the gas phase ($mol \cdot m^3$)
k_{26}^{rad} = rate constant for radiation-induced RI formation
k_{26} = rate constant for thermal-induced RI formation
[DEP] = iodine deposited on paint (both dry and submerged) ($mol \cdot m^2$)
A = total (submerged and dry) painted surface area (m^2)
V_g = gaseous volume (m^3)
k_{dec} = rate constant for decomposition of organic iodide (gas phase)
D = dose rate ($kGyh^{-1}$)

The production of organic iodides from this process is virtually independent of temperature up to about 100°C (i.e., $k_{26}^{rad} > k_{26}$); thermal processes contribute at higher temperatures. The overall production rate is somewhat dependent upon pH, since the concentration of I_2 in either the gas or aqueous phase has some effect on the amount of iodine deposited on the surfaces. INSPECT also incorporates hydrolysis and radiolytic decomposition of CH_3I in the aqueous phase in the same way as IMPAIR. As is the case for IODE(IPSN) and IMPAIR, the predicted dose rate dependence of the rate of production of organic iodides in INSPECT could be much greater than in IMOD or LIRIC, depending on whether the amount of iodine deposited on the surfaces is a function of the dose rate.

2.3 Deposition of Iodine on Ag

All of the codes have a similar model for the deposition of iodine on silver surfaces. Deposition is treated as a first-order process, dependent upon the surface area of the Ag:

$$I_2 + 2Ag \rightarrow 2AgI \quad (28)$$

$$d[AgI]/dt = k_{28}[I_2]A_{Ag}/\, V_{aq} \quad (29)$$

where A_{Ag} (m^2) is the total surface area of Ag, and V_{aq} (m^3) is the aqueous phase volume.

IODE(IPSN) and INSPECT also include a two-step reaction, in which a fraction of the silver becomes oxidized and reacts with I^- to produce AgI:

$$Ag \rightarrow Ag_{ox} \quad \text{slow} \quad (30a)$$

$$Ag_{ox} + I^- \rightarrow AgI \quad \text{fast} \qquad (30b)$$

$$d[Ag_{ox}]/dt = k_{30a} A_{Ag}/V_{aq} - k_{30b} [I^-] A_{ox}/V_{aq} \qquad (31)$$
$$d[AgI]/dt = k_{30b} [I^-] A_{ox}/V_{aq} \qquad (32)$$

where A_{ox} is the area of oxidised silver (m^2), V_{aq} is the aqueous volume (m^3), and A_{Ag} is the total surface area (m^2) of silver. If A_{ox} is less than A_{Ag}, then the kinetics of silver oxidation determine the rate of iodide reaction with Ag_{ox}, with $d[Ag]/dt = - k_{30a} A_{Ag}/V$ and $d[AgI]/dt = k_{30b} [I^-] A_{ox}/V$. If A_{ox} is greater than or equal to A_{ag}, then an oxide layer surrounds the silver particle and the reaction corresponds to the reaction of iodide ions with the silver oxide. The kinetics are determined by the mass transfer of iodide ions to the Ag particle surface and are therefore first-order relative to iodide. The rate of Reaction (30a) is pH-dependent, with the pH dependence of k_{30} being user-defined.

In IMPAIR, I^- is assumed to react directly with Ag in one step, and the reaction is independent of pH:

$$Ag + I^- \rightarrow AgI(s) \qquad (33)$$

2.4 Gas-Phase Reactions

Another difference between the codes is the participation of gas-phase reactions or reactants. Reactions of particular importance involve the production of nitric acid by the radiolysis of air, for the calculation of pH in IODE(IPSN) and the gas phase reaction between molecular iodine and ozone to form iodate in IMPAIR. In IODE(IPSN), nitric acid production and the release of CO_2 from molten core concrete interactions (MCCI) into containment are responsible for the pH changes that are induced when pH is not controlled (see Case 5 calculations, Appendix C). The release of CO_2 is provided as an input to IODE(IPSN) from upstream calculations, whereas nitric acid formation is calculated within the code using a G-value, which results in a linear increase in nitric acid concentration as a function of time.

The iodate formation reaction incorporated in IMPAIR is

$$I_2(g) + 2O_3(g) \rightarrow 2IO_3^-(g) \qquad (34)$$

The reaction is modelled as a first-order decomposition of I_2, with a rate constant of 1.1×10^{-4} s^{-1}. The removal of iodate aerosol by absorption into steam, or by aerosol removal mechanisms is not modelled in the current exercise. Reaction (34) results in IMPAIR predicting that a significant fraction of the iodine inventory is converted to iodate over the course of several hours. Note that Reaction (34) is also included in IODE(IPSN), but was not used in this exercise.

2.5 Interfacial Mass Transfer and Surface Adsorption

Mass transfer and surface adsorption (excluding adsorption on Ag) are modelled in a similar manner in all of the codes. The approach uses a standard two-resistance model. The values recommended for this exercise for the mass transfer coefficients and partition coefficients can be found in Appendix A. The adsorption of I_2 on containment surfaces (both wet and dry) is described as a first-order process, with recommended rate constants as given in Appendix A. Some of the codes also provide the option of modelling I^- absorption in the aqueous phase, and IMPAIR calculations used this option for this exercise.

2.6 Condensation

The effect of the condensation of steam on iodine volatility is modelled in LIRIC and IMOD using a two-step kinetic scheme. Molecular iodine (but not organic iodides) is assumed to be absorbed into a condensing film covering the surfaces, in a simple first-order process that is identical to that of absorption. Once absorbed into the condensing steam, it is assumed to be hydrolysed to I^- and returned to the sump by the condensate flow. The absorption of molecular iodine on non-immersed surfaces in the presence of steam is assumed to be slower than its absorption on the same surfaces under non-condensing conditions:

$$\frac{d([I_2(con)])}{dt} = k_{AD}^{cw} \cdot [I_2(g)] \cdot \frac{V_g}{V_{con}} \quad (35)$$

$$\frac{d([I_2(g)])}{dt} = -k_{AD}^{cw} \cdot [I_2(g)] \quad (36)$$

where V_{con} is the volume of the condensate on the wall in dm^3, V_g is the volume of the gas phase, and k_{AD}^{CW} is the rate constant for the absorption of iodine in condensing water. k_{AD}^{CW} is further defined as

$$k_{AD}^{CW}\ (s^{-1}) = v_{AD}^{CW} \cdot (A_{con}/V_g) \quad (37)$$

$$v_{AD}^{CW}\ (dm \cdot s^{-1}) = (7 \pm 2) \times 10^{-4} \quad (38)$$

where A_{con} is the surface area of the condensing water film in units of dm^2.

The mass transport rate of iodine from wall condensate to the aqueous phase depends on the condensation rate of water, therefore, it depends on the steam concentration, the temperature difference between the gas phase and the wall, and to a minor extent, the type of surface. The process is incorporated as a first-order process in both models:

$$\frac{d([I_2(con)])}{dt} = -k_{con} \cdot [I_2(con)] \quad (39)$$

$$\frac{d([I^-(aq)])}{dt} = 2\ k_{con} \cdot [I(con)] \cdot \frac{V_{con}}{V_{aq}} \quad (40)$$

$$k_{con}\ (s^{-1}) = F_{con}/V_{con} \quad (41)$$

where F_{con} is the flow rate of condensate going into the aqueous phase ($dm^3 \cdot s^{-1}$), and V_{con} is the volume of condensate on the walls in dm^3. Recommended values for V_{con} and F_{con} can be found in Appendix A.

In IODE(NRIR), IODE(IPSN), INSPECT and IMPAIR, the fraction of gaseous iodine removed by condensation and transported to the bulk water phase is assumed to be the same as the fraction of the mass of steam that is condensed into the bulk phase. These codes assume that organic iodides are also removed by steam condensation, whereas LIRIC and IMOD do not. They also differ from LIRIC and IMOD in that they do not assume that I_2 and CH_3I are hydrolysed to I^-; rather, these species remain in the same form when they are transferred to the bulk water phase.

Regardless of the model used, the condensation sub-model results in a first-order rate of removal of gaseous iodine species from the gas phase.

3. RESULTS AND DISCUSSION

3.1 The Effect of Boundary Conditions on Iodine Volatility

The following sections summarize some of the trends that are observed in code predictions of the percentage of the iodine inventory in the gas phase, as a result of changing input parameters (initial conditions) for various cases (see Appendix A). Note that the percentage of the iodine inventory in the gas phase for IMPAIR shown in the figures does not include iodate (IO_3^-) as an aerosol species produced by the reaction of I_2 with O_3, whereas the mass balances presented in Appendix B include iodate. Note also that all of the results shown below were taken from code predictions at 25 h rather than at 75 h. This was done because at pH 5, most of the codes predicted that the iodine inventory would be almost entirely deposited on surfaces by 75 h. With only a fraction of the iodine inventory in the aqueous phase as I^-, the rate of production of volatile iodine species is much smaller at 75 h than at 25 h, and the fraction of the iodine inventory in the gas phase is significantly reduced.

The Effect of Dose Rate

The effect of dose rate on iodine volatility at pH 9 and pH 5, as predicted by the various codes, is shown in Figures 1 and 2.

The relationship between dose rate and iodine volatility in each of the codes is quite complex. In LIRIC and INSPECT, the dose rate affects the steady-state concentration of •OH, the species responsible for the oxidation of non-volatile I^- to volatile I_2, and also affects the steady-state concentrations of H_2O_2, O_2^- and e^-_{aq}, which reduce volatile I_2 and CH_3I to non-volatile I^-. The balance between oxidant and reductant concentrations is dependent upon the pH (e.g., the pK_a of $HO_2 = H^+ + O_2^-$ is 4.8) and the presence of impurities, such as organic compounds. The two codes are slightly different in their predictions; however, they both predict a modest (less than a factor of 10) increase in iodine volatility as the dose rate is increased by a factor of 100 at both pH values.

IODE(IPSN) and IODE(NRIR) predict that iodine volatility will increase linearly with an increase in the dose rate at pH 9. This prediction is understandable in view of the fact that IODE models the rate of production of I_2 from I^- (Reaction (8)) as having a linear dependence on dose rate. In both codes, the production of organic iodides from painted surfaces has a dose rate dependence as well. Neither IODE(IPSN) nor IODE(NRIR) assumes that organic iodides are decomposed radiolytically. As a consequence, both codes predict significant increases in iodine volatility with an increase in dose rate. The results of IODE(IPSN) predictions at pH 5 are complicated by the fact that by 25 h, particularly at $10 kGy \cdot h^{-1}$, most of the iodide in the aqueous phase has been depleted due to volatilization and adsorption, and the rate of production of volatile iodine species decreases as the amount of I^- in the aqueous phase decreases. This process results in iodine volatility at 25 h being much less than would be expected at earlier stages.

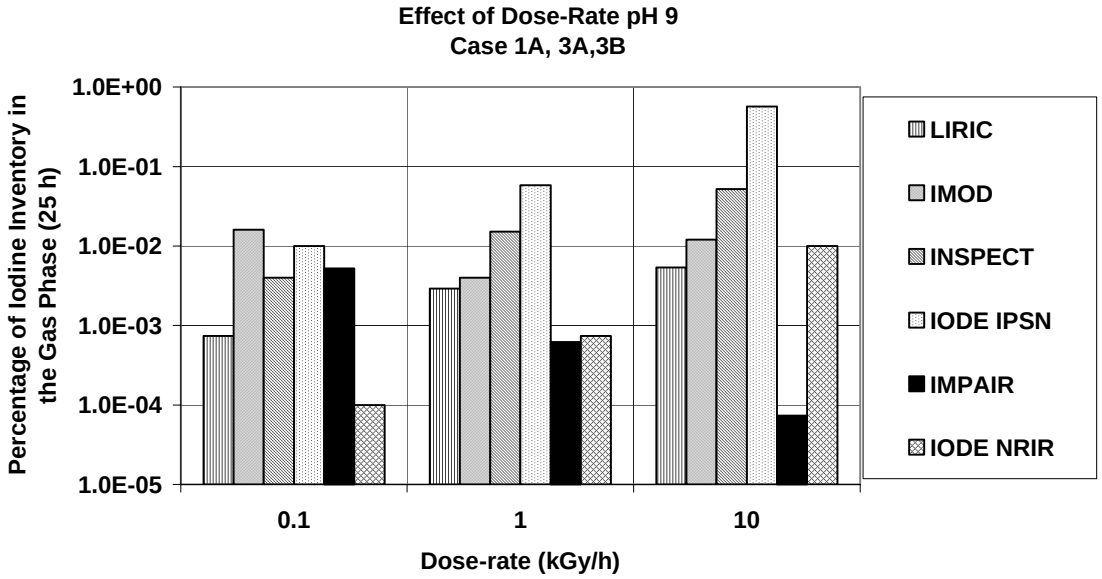

Figure 1. The effect of dose rate on the percentage of iodine inventory in the gas phase at 25 h for a solution initially containing 1×10^{-5} mol·dm^{-3} CsI at 90°C and pH 9.

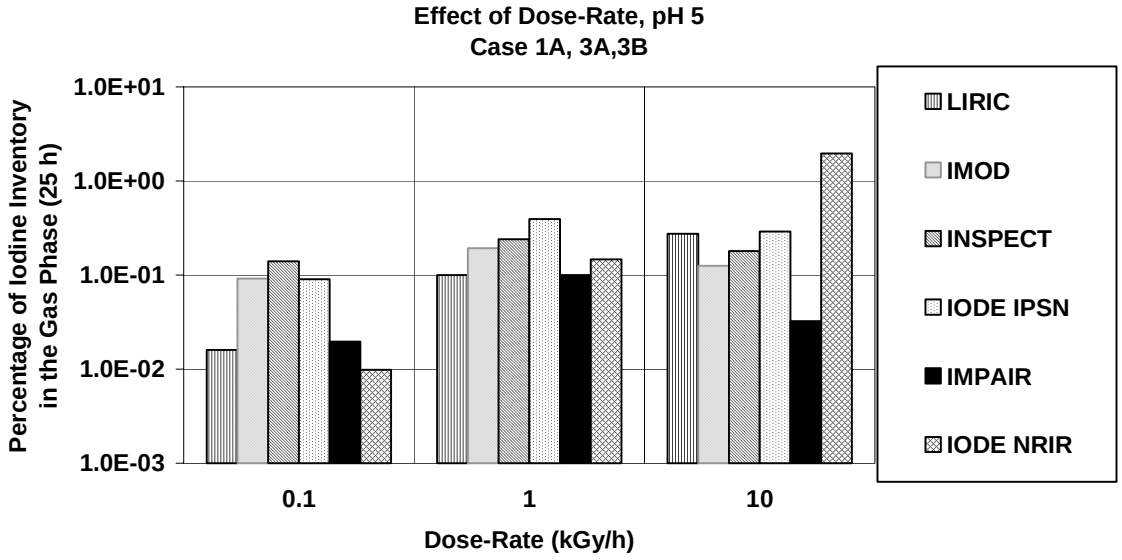

Figure 2. The effect of dose rate on the percentage of iodine inventory in the gas phase at 25 h for a solution initially containing 1×10^{-5} mol·dm^{-3} CsI at 90°C and pH 5.

The Effect of pH

The pH of the aqueous phase is one of the most important factors that influences the volatility of iodine species. The effect of aqueous pH on iodine volatility at 25 h, as predicted by each of the iodine behaviour codes for aqueous solutions irradiated at 90°C and at a dose rate of 1 kGy·h^{-1}, is shown in Figure 3.

The predicted fraction of the iodine inventory in the gas phase at 25 h, as a function of pH, varies dramatically from code to code. LIRIC and IMOD predict an increase of a factor of about 50 in iodine volatility in going from pH 9 to pH 5 (this would vary depending on the temperature), whereas IODE(IPSN) and INSPECT predict an increase of about a factor of 5 and 10, respectively. IODE(NRIR) and IMPAIR predict that iodine volatility will be higher at pH 5 than at pH 9 by a factor of about 500.

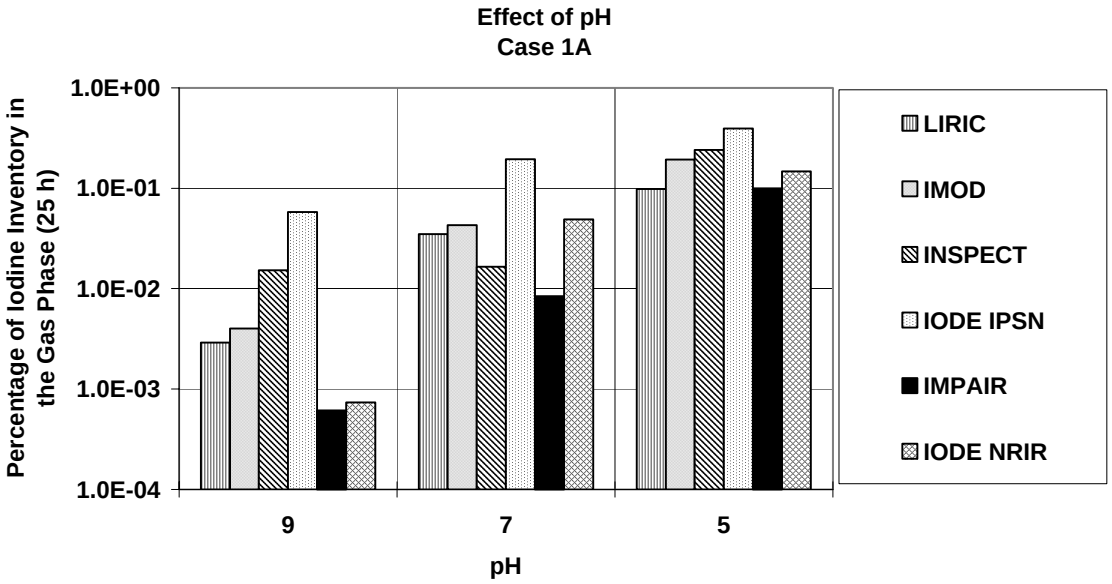

Figure 3. The effect of pH on the percentage of iodine inventory in the gas phase at 25 h for a solution initially containing 1×10^{-5} mol·dm^{-3} CsI at 90°C and irradiated at a dose rate of 1 kGy·h^{-1}.

It is not surprising that there are some differences between the codes in their predictions of the gaseous iodine fraction at a given pH. The interconversions between non-volatile and volatile iodine species are modelled slightly differently in each code. For example, as outlined in Section 2.1, in LIRIC, IMOD and INSPECT, the rate of reduction of volatile I_2 and organic iodides to non-volatile I^- increases with increasing pH (Reactions (1–3), (6), (7)), whereas the rate of production of I_2 (Reaction (5)) is pH-independent. The **overall** rate of formation of volatile iodine species as calculated by each of these codes should therefore be inversely proportional to the pH—this is what is observed. From Figure 3, there is a stronger pH

dependence in IMOD and LIRIC than in INSPECT; nevertheless, the codes are qualitatively in agreement.

In IODE(NRIR), IODE(IPSN) and IMPAIR, the rate of production of all volatile iodine species (including organic iodides) is inversely dependent on the aqueous pH (Reactions (8), (20), (22)), and the rate of decomposition of these species is pH-independent. The pH dependence of iodine volatility predicted by these codes could potentially be larger than that predicted by IMOD, LIRIC and INSPECT, because organic iodide formation has a direct pH dependence. As expected, based on the I_2 and RI production rates, all the codes predict the same **overall** effect of pH on iodine volatility. Nonetheless, the sensitivity of the iodine volatility to pH changes does vary considerably, because the rate of production of I_2 in each code (Reaction (8)) is defined by Equation (10), which has adjustable, user-defined parameters. The choice of parameters used in Equation (10) can substantially change the sensitivity of iodine volatility to pH.

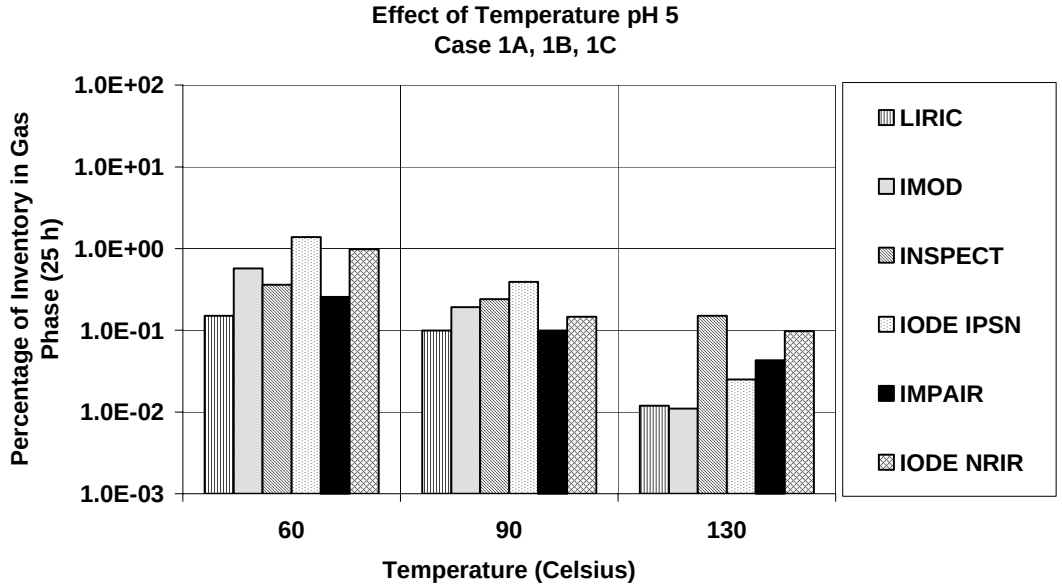

Figure 4. The effect of temperature on the percentage of iodine inventory in the gas phase at 25 h for a solution initially containing 1×10^{-5} mol·dm^{-3} CsI at pH 5 and irradiated at a dose rate of 1 kGy·h^{-1}.

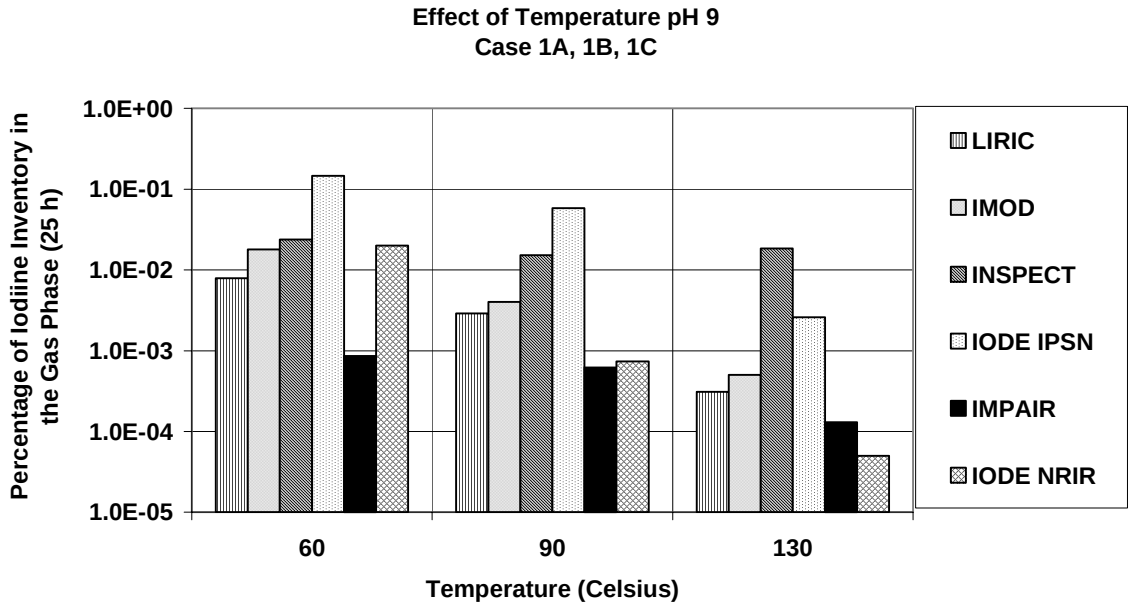

Figure 5. The effect of temperature on the percentage of iodine inventory in the gas phase at 25 h for a solution initially containing 1×10^{-5} mol·dm^{-3} CsI at pH 9 and irradiated at a dose-rate of 1 kGy·h^{-1}.

The Effect of Temperature

The predicted effect of temperature on the fraction of the iodine inventory in the gas phase is shown in Figures 4 and 5. Most of the codes predict that an increase in temperature from 60 to 130 °C will result in a decrease in the fraction of iodine in the gas phase, both at high and low pH.

The effect of temperature on iodine volatility depends upon the balance between the temperature dependence of the production and depletion rates of volatile iodine species, and the partitioning of these species. All of the codes incorporate a temperature dependence on the partitioning of volatile iodine species, resulting in I_2 and organic iodides being more volatile at higher temperatures. The recommended temperature dependence for the equilibrium-partitioning coefficient of volatile iodine species for this exercise can be found in Appendix A.

All of the codes also incorporate a temperature dependence for the iodine hydrolysis equilibrium (Reactions (1–3)) resulting in I_2 being hydrolysed more rapidly to non-volatile HOI and I^- at higher temperatures. Other temperature-dependent reactions that reduce iodine volatility as temperature increases are the hydrolysis of organic iodides and the adsorption of iodine on surfaces. In general, in going from 60 to 130ºC, the temperature dependence of the depletion rate of volatile iodine species more than compensates for the increase in their volatility, with the result that most of the codes predict that there will be less iodine in the gas phase at the higher temperature. INSPECT predictions at pH 9 are the exception. The temperature dependence of

Reaction (26) in INSPECT, which predicts that organic iodide production will increase with increasing temperature at about 100°C, is likely responsible for this trend.

The Effect of Iodide Concentration

The semi-empirical codes IODE(NRIR), IODE(IPSN), IMPAIR and IMOD predict that the percentage of the iodine inventory in the gas phase is nearly independent of the initial iodide concentration, whereas LIRIC and INSPECT show a decrease in the percentage, with an increase in iodide concentration (see Figures 6 and 7). INSPECT predicts a significant (greater than a factor of 10) decrease in the percentage of iodine in the gas phase, as a result of an increase in iodide concentration by two orders of magnitude, at pH 9. At pH 5, INSPECT predicts a decrease in the gas-phase percentage as the iodide concentration is increased from 10^{-5} to 10^{-4} mol·dm^{-3}, following a slight increase in iodine volatility due to an increase in iodide concentration from 10^{-6} to 10^{-5} mol·dm^{-3}. LIRIC predicts a very small decrease in the gas-phase fraction as the iodide concentration is increased at pH 5, and a slightly more significant decrease at pH 9.

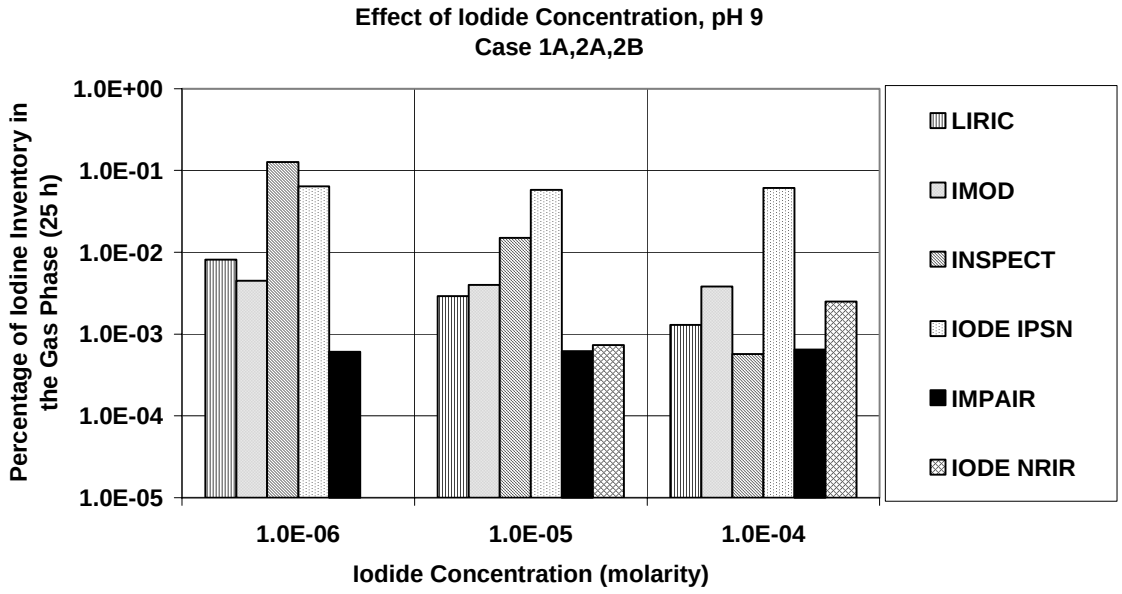

Figure 6. The effect of iodide concentration on the percentage of iodine inventory in the gas phase at 25 h for a solution initially containing CsI at pH 9 and 90ºC irradiated at a dose rate of 1kGy·h^{-1}. Note that IODE(NRIR) calculations were not performed for 1×10^{-6} mol·dm^{-3} I$^-$.

In IODE(NRIR), IODE(IPSN), IMOD and IMPAIR, the rate of production of I_2 is directly proportional to the iodide concentration (Reaction (8)). In addition, all of these codes formulate the production of organic iodides as being either directly or indirectly dependent on the iodide concentration. Therefore, regardless of whether organic iodides or I_2 dominates amongst gaseous

iodine species, an increase in the iodide concentration by a factor of 10 should result in all of these codes predicting about[4] a factor of 10 increase in the gas-phase iodine concentration—the fraction (or percentage) of the iodine inventory in the gas phase would remain unchanged. This behaviour is observed in Figure 7.

In LIRIC and INSPECT, the predicted steady-state concentration of volatile iodine species in the aqueous phase depends upon the ratio of the oxidation rate of iodide to I_2 by •OH radicals (Reaction (5)) to the conversion rate of I_2 and RI to non-volatile species by hydrolysis and radiolysis ((Reactions (1–3), (6), (7), (17), (18)). These codes differ from the semi-empirical codes, in that an increase in I^- concentration does not result in a proportional increase in the rate of production of I_2, because an increase in I^- concentration also serves to decrease the steady-state concentration of •OH, i.e., the species responsible for oxidizing iodide to I_2.[5] Based on the rate of formation of I_2 alone, an increase in iodide concentration by a factor of ten would result in less than a factor of ten increase in the concentration of I_2 in the aqueous or gas phase, and a small decrease in the percentage of iodine inventory in the gas phase.

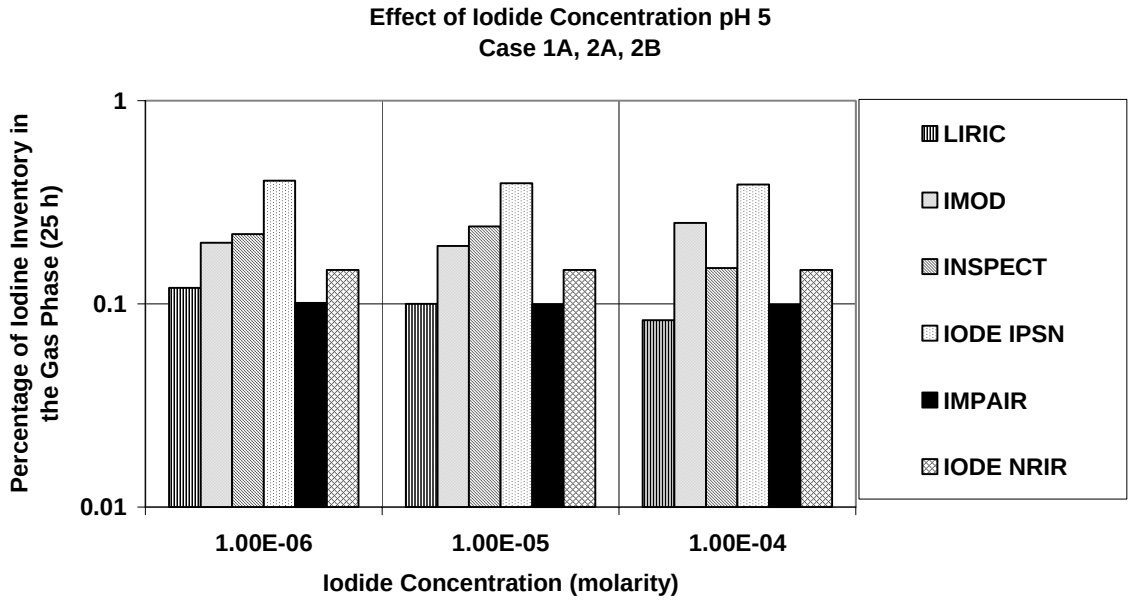

Figure 7. The effect of iodide concentration on the percentage of iodine inventory in the gas phase at 25 h for a solution initially containing CsI at pH 5 and 90ºC irradiated at a dose rate of 1 kGy·h^{-1}.

[4] A small dependence of the percentage on the initial iodide concentration may be observed in these codes, if the contribution of the iodine hydrolysis equilibrium (Reaction (1)) to the conversion of non-volatile iodine species to I_2 is significant.

[5] At 1 kGy·h^{-1}, the steady-state concentration of •OH is significantly decreased, when iodide concentrations approach about 10^{-4} mol·dm^{-3}. Also, the •OH concentration is decreased by the presence of organic impurities. Therefore, the overall rate of production of I_2 may not increase linearly with an increase in iodide concentration.

In LIRIC and INSPECT, the depletion of I_2 in the aqueous phase is also dependent upon iodide concentration. The hydrolysis equilibrium (Reaction (1)) dictates that an increase in iodide concentration decreases the rate of depletion of I_2 by hydrolysis, and increases iodine volatility. The depletion of I_2 by O_2^- (Reaction (6)) has the opposite iodide dependence, because an increase in iodide concentration increases the O_2^- concentration. For LIRIC and INSPECT predictions under acidic or neutral (pH 4-7) conditions, the iodide dependence of the hydrolysis equilibrium offsets the dependence of the rate of formation of I_2; the codes predict that the gaseous iodine fraction changes only slightly with iodide concentration. At high pH values, however, the iodine hydrolysis equilibrium (Reaction (3)) lies so far to the right (i.e., it favours the formation of I^- and HOI), that it becomes virtually independent of iodide concentration. At pH 9, the iodide dependence of the percentage of iodine inventory in the gas phase is what would be expected based on the dependence of the I_2 formation rate on iodide concentration. This iodide dependence is further augmented by the iodide dependence of O_2^- reduction. Therefore, at pH 9 and 90ºC, LIRIC and INSPECT predict that an increase in iodide concentration will more substantially decrease the percentage of the iodine inventory in the gas phase.

The Effect of Condensation

The effect of condensation on iodine volatility at pH 5, as predicted by each of the codes, is shown in Figure 8. IMPAIR, LIRIC and IMOD predict that the presence of condensing steam will increase iodine volatility, whereas INSPECT, IODE(IPSN) and IODE(NRIR) predict that it will decrease the gaseous iodine fraction. The qualitative predictions of each of the codes at pH 9 are the same as for pH 5.

Code predictions regarding the effect of condensing steam on iodine volatility depend on whether the rates for removal of airborne iodine by condensation (i.e., absorption into the condensate, and return flow to the sump) are faster or slower than the rates of removal of iodine by absorption onto surfaces in the absence of condensation. In LIRIC, IMOD and IMPAIR, the default rate constants for the removal of iodine from the gas phase are such that iodine is removed more slowly in the presence of condensation than under dry conditions. That is, the overall rate for the deposition of iodine, which encompasses absorption into a condensing film, and absorption onto surfaces in contact with the condensing film, is lower than the rate constant for deposition onto dry surfaces. As a result, these codes predict that less iodine is lost to the surfaces in the presence of condensing steam, and that the gaseous fraction increases. On the other hand, IODE(IPSN), IODE(NRIR) and INSPECT predict that the rate of removal of gaseous iodine species to the surfaces is enhanced by condensation, because this process enhances the mass flux to the surface. As a result, these codes predict a decrease in iodine volatility as a result of condensation. Note that the effect is quite small for all of the codes.

[6] At 1 $kGy \cdot h^{-1}$, the steady-state concentration of •OH is significantly decreased, when iodide concentrations approach about 10^{-4} $mol \cdot dm^{-3}$. Also, the •OH concentration is decreased by the presence of organic impurities. Therefore, the overall rate of production of I_2 may not increase linearly with an increase in iodide concentration.

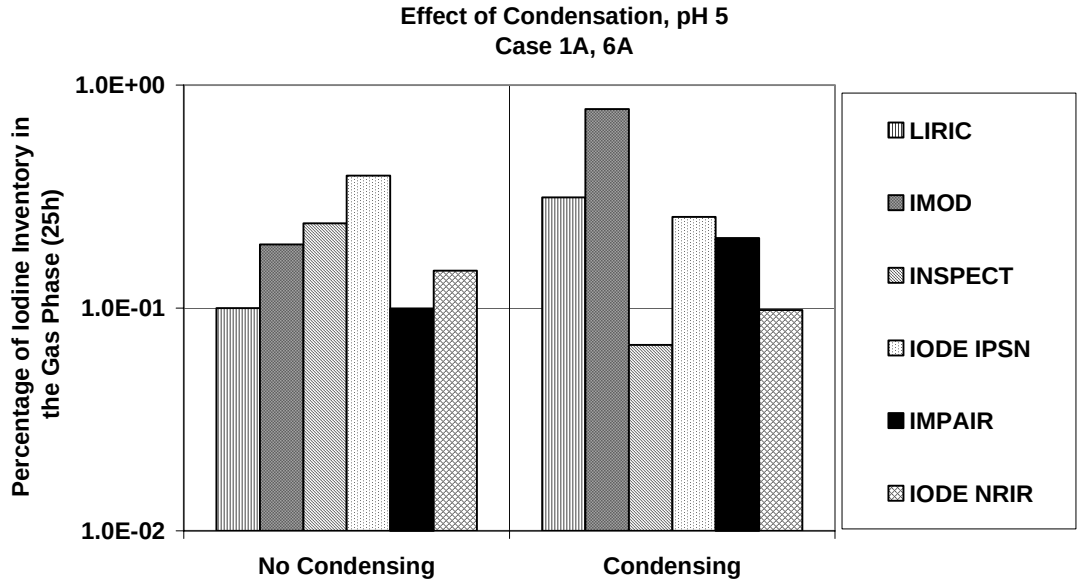

Figure 8. The predicted effect of condensing steam on the percentage of iodine inventory in the gas phase at 25 h for a solution initially containing 1×10^{-5} mol·dm^{-3} CsI at pH 5 and 90°C irradiated at a dose rate of 1 kGy·h^{-1}.

The Effect of Silver

The effect of the presence of silver in the sump, as predicted by each of the codes, is shown in Figure 9.

As would be expected, all of the codes predict that iodine volatility is reduced when silver is present. However, the magnitude of the decrease in volatility varies quite dramatically. For the conditions used in Figure 9, for example, IMPAIR predicts that the presence of silver would reduce iodine volatility almost imperceptibly, whereas in IODE(IPSN), the predicted amount of iodine in the gas phase is reduced by four orders of magnitude.

Some of the differences between code predictions can be attributed to the different mechanisms that are assumed for iodine adsorption on Ag. For example, both IODE(IPSN) and INSPECT assume that AgO reacts with I^-, with AgO being formed from Ag in a pH-dependent process. LIRIC, IMOD and IODE(NRIR), on the other hand, assume that only I_2 reacts with Ag. However, the effect of Ag on iodine volatility is also dependent upon the amount of various iodine species calculated by each code. IODE(IPSN) and INSPECT both assume that iodide reacts with AgO (Reaction (30b)) and that I_2 reacts with Ag (Reaction (28)). These codes use the same rate constants for reactions between silver species and iodine species, yet their predictions of iodine volatility in the presence of Ag are quite different. This discrepancy occurs because the codes differ in their predictions regarding the rates of formation and destruction of I_2 (Reactions (5) and (8)), the processes that determine the concentrations of I_2 and I^- that will be reacting with silver species.

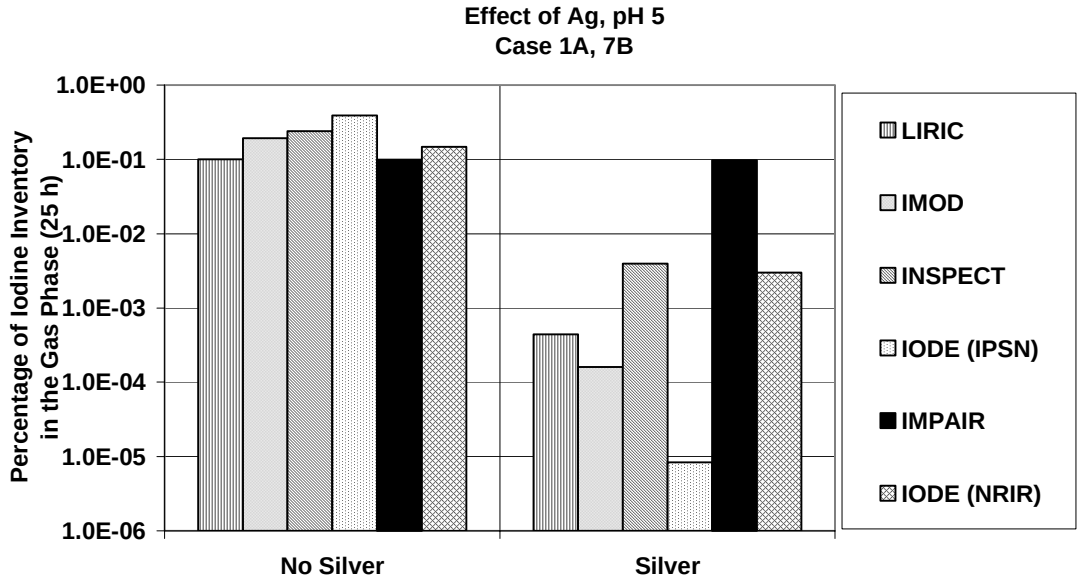

Figure 9. The predicted effect of Ag in the aqueous phase on the percentage of iodine inventory in the gas phase at 25 h for a solution initially containing 1×10^{-5} mol·dm^{-3} CsI at pH 5 and 90ºC irradiated at a dose rate of 1kGy·h^{-1}.

IMPAIR predicts that Ag will have a negligible impact on iodine volatility for three reasons. Firstly, in IMPAIR, I_2 is converted rapidly to IO_3^- in the gas phase; a much smaller fraction of iodine is present in the aqueous phase (as I_2) than in the other codes. Secondly, the rate constant used for the reaction between I_2 and Ag is smaller in IMPAIR (2.2×10^{-6} m·s^{-1}) than in IODE, IMOD and LIRIC (1×10^{-5} m·s^{-1}). Finally, IMPAIR does not consider Ag_2O as a reactive species, and assumes that Ag reacts with I^- at a relatively slow rate.
(2.2×10^{-6} m·s^{-1}). Consequently, much less of the iodine inventory is retained by Ag in IMPAIR, and the gaseous iodine fraction is not influenced as much by the presence of Ag as it is in the other codes.

The Effect of Organic Impurity Concentrations

The effect of an initial organic impurity concentration on the iodine volatility predicted by each code is shown in Figure 10. Note that the calculations presented in Figure 10 for IODE(NRIR) for 1×10^{-3} mol·dm^{-3} organic impurity are the same as the calculations of these codes for Case 1A, in which the organic impurity concentration is user-defined. IODE(NRIR) already assumes an initial organic impurity level of about 1×10^{-3} mol·dm^{-3}; therefore, the conditions used to generate Figure 10 are qualitatively the same as those used for Case 1A. There are no INSPECT calculations for this case, because INSPECT does not include a homogeneous aqueous-phase mechanism for the formation of organic iodides.

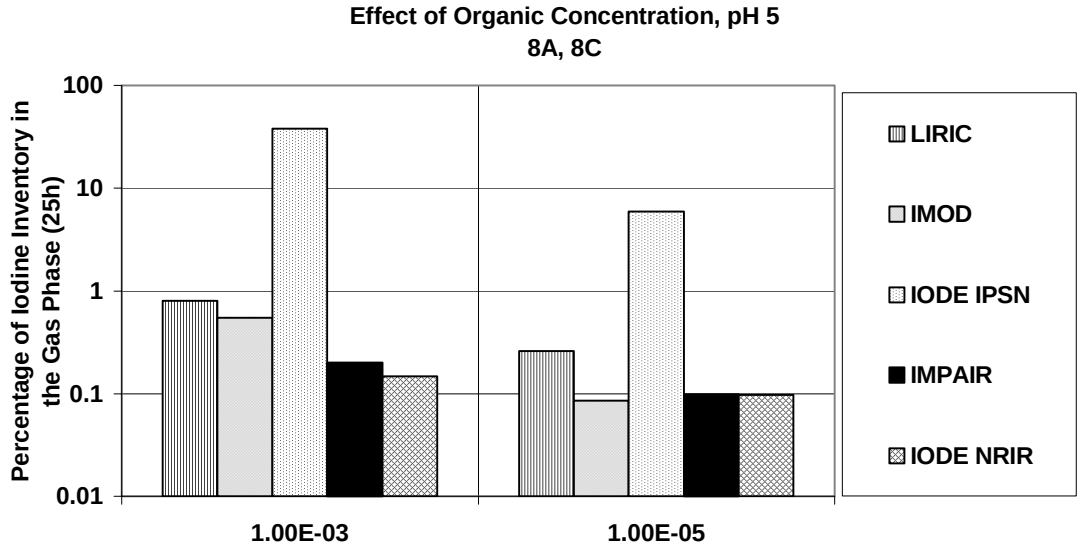

Figure 10. The predicted effect of organic impurities in the aqueous phase on the percentage of iodine inventory in the gas phase at 25 h for a solution initially containing 1×10^{-5} mol·dm^{-3} CsI at pH 5 and 90ºC irradiated at a dose rate of 1 kGy·h^{-1}.

In general, the codes predict that an increase in organic impurity concentration results in an increase in the amount of iodine in the gas phase. This can be rationalized in view of the fact that the rate of production of organic iodides from homogeneous aqueous-phase processes (Reactions (16) and (20)) is dependent upon the concentration of organic radicals in the aqueous phase, and this concentration should, in turn, be dependent upon the concentration of organic impurities in the sump. In all of the codes, organic iodide production by homogeneous aqueous-phase processes results in only a small fraction of the I_2 produced being converted to organic iodides, and I_2 is the dominant volatile species that is produced. However, I_2 is easily absorbed on surfaces, whereas organic iodides are not. Once partitioned into the gas phase, organic iodides persist as volatile species, whereas I_2 is rapidly removed by absorption. As a result, most of the codes predict that a large fraction of the gaseous iodine inventory is in the form of organic iodides, and the total iodine concentration in the gas phase is dependent on the rate of the organic iodide formation in the aqueous phase.

pH Predictions

Only LIRIC, IMOD and IODE(IPSN) have the option of performing calculations to model pH behaviour in unbuffered solutions. An example of the predictions of each of the codes is shown in Figure 11 for a solution containing 1×10^{-5} mol·dm^{-3} CsI at 90°C, irradiated at a dose rate of 10 kGy·h^{-1}.

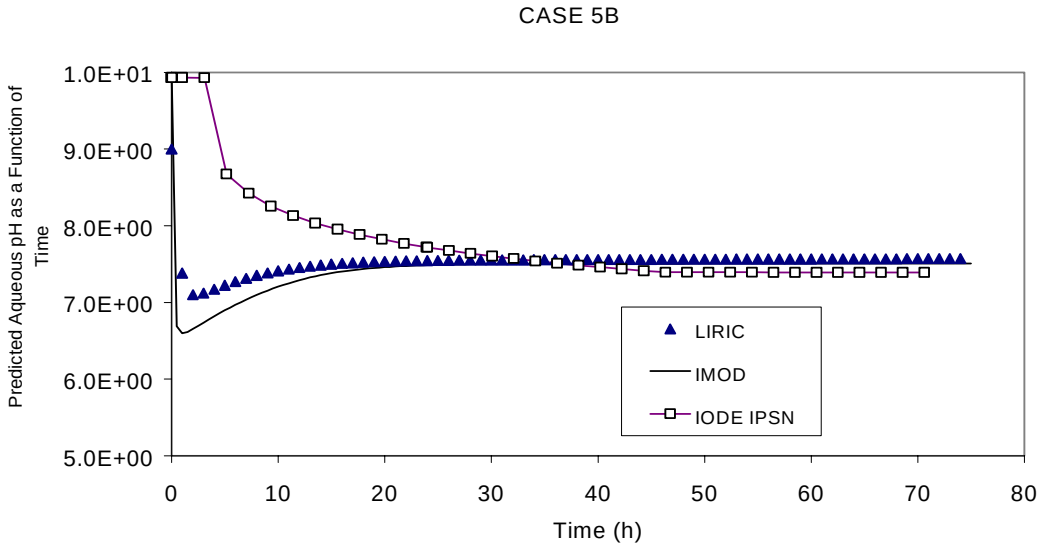

Figure 11. The pH of irradiated (10 kGy·h^{-1}) containment sump water initially containing 1×10^{-5} mol·dm^{-3} CsI at pH 5 and at 90ºC as predicted by LIRIC, IMOD, and IODE(IPSN). The sump water is assumed to be in contact with painted surfaces.

As would be expected, LIRIC and IMOD predict very similar pH profiles. The reactions and rate constants that induce pH changes (i.e., the release of organic compounds into the aqueous phase (Reaction (19)) and their subsequent radiolytic decomposition (Reactions (14), (15))) in these models are virtually identical. IODE(IPSN) predicts a more modest rate of decrease in aqueous pH initially, because the pH model in IODE(IPSN) takes into account the buffering effects of boron released from safety systems and CO_2 release from MCCI as well as the formation of nitric acid from air and ozone interaction. The final pH value predicted by IODE(IPSN) is similar to that obtained by LIRIC and IMOD, because a buffering effect of CO_2 is predicted by all codes. Results obtained using dose rates of 1 kGy·h^{-1} and 0.1 kGy·h^{-1} are qualitatively similar; the radiolysis of organic materials to organic acids as modelled by LIRIC and IMOD has a greater impact on aqueous pH than does the cumulative effect of nitric acid formation and the release of CO_2 from the MCCI in IODE(IPSN).

Effect of a Programmed pH Drop

Figure 12 shows the effect of rapidly decreasing pH on iodine volatility, as predicted by each of the codes. Most of the codes predict similar kinetic behaviour, with the gas-phase iodine concentration increasing rapidly as the pH decreases. The gas-phase iodine concentration is also, in most cases, predicted to reach a maximum value, followed by a slow decrease as I_2 is adsorbed on surfaces. The strange behaviour of the gas-phase concentration predicted by LIRIC is an artefact of the way in which the pH values were provided as input.

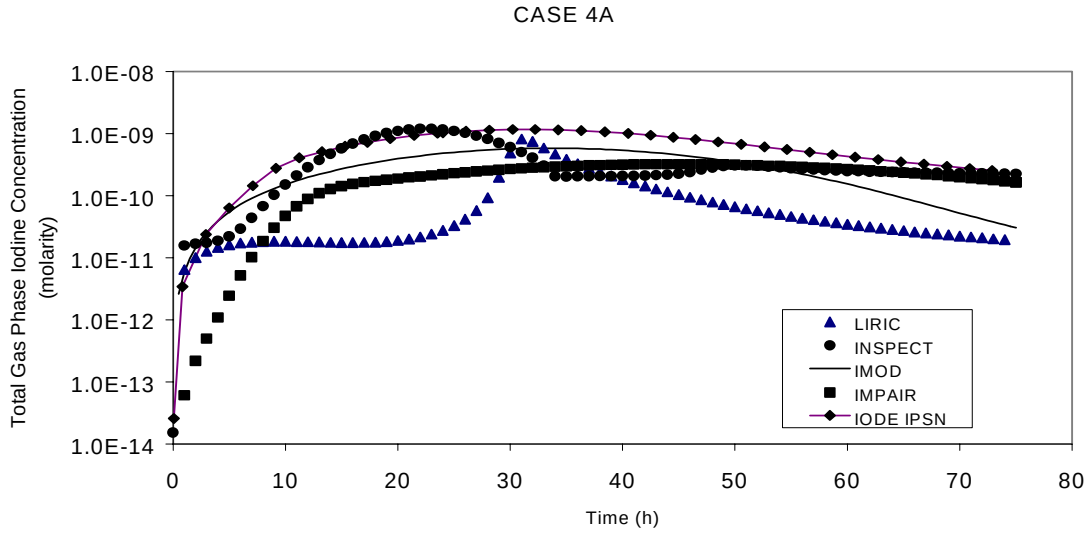

Figure 12. The total iodine concentration in the gas phase from an irradiated (1 kGy·h^{-1}) solution initially containing 1×10^{-5} mol·dm^{-3} CsI and at 90ºC, as predicted by the iodine behaviour codes. The pH is assumed to start at 10, and then drop to around 3.5 in 75 h.

FACSIMILE[7], the commercial differential equation solver used to solve the kinetics of the reactions described in LIRIC, uses an integration method that assumes that variables are smooth functions over time, and estimates a polynomial approximation for the values of the variables over a large integration step. When one introduces a large step change in one variable or parameter (e.g., a pH drop from 10 to 9.5), the FACSIMILE approximation for changes in the concentration of other variables (e.g., water radiolysis product concentrations) is less accurate than when only small changes in input parameters are made. The application of several consecutive large perturbations to the pH values results in a significant time lag between the pH being changed and the I_2 concentrations responding to the change. This effect can be seen in Figure 13. When a pH change is input every ½ h, the gaseous iodine concentration remains the same for the first 20 h, even though the pH drops significantly over the same time period. As the pH input is increased in frequency, and the pH steps become smaller, the amount of time required for species concentrations to reach a steady state decreases, and the time lag between a pH change and an increase in iodine volatility gets progressively smaller. Presumably, if the pH was provided as input every second or fraction of a second, then a smooth concentration profile would be observed for the gaseous iodine concentration, similar to that predicted by the other models.

[7] The FACSIMILE program is a commercial integration package (AEA Technologies, Harwell, UK) for solving coupled-differential equations that was specifically designed for chemical systems. The chemical system to be modelled is expressed as a series of simple chemical reactions, which is then converted into coupled differential equations and solved by FACSIMILE's numerical integration method.

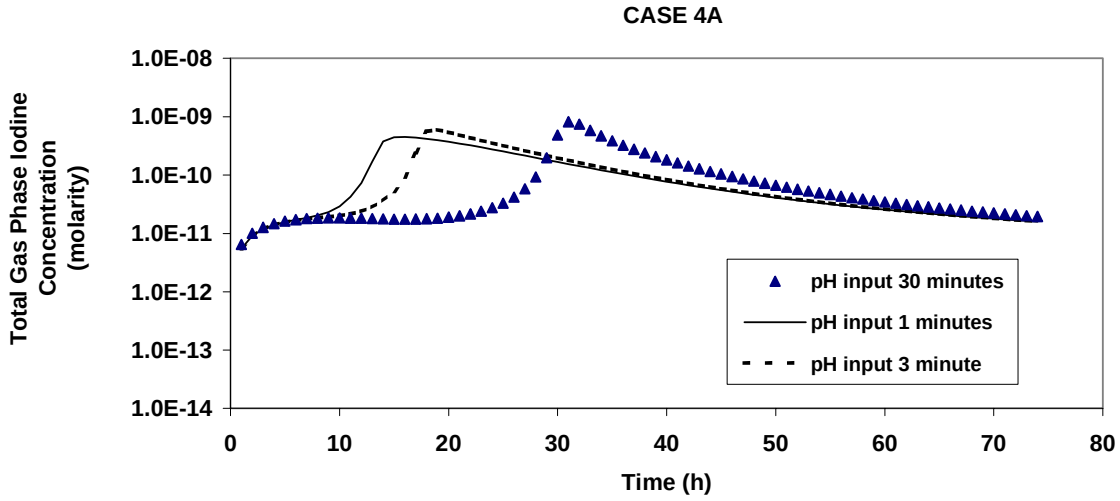

Figure 13. Predicted concentration of iodine species in the gas phase from a containment sump initially containing 1×10-5 mol·dm-3 CsI solution (1 kGy·h-1, 90ºC). The pH is assumed to start at 10, and then drop to around 3.5. The effect of various time steps for pH input is shown.

The LIRIC results shown in Figure 13 are a clear demonstration that care must be taken in the way in which user-defined input is provided to models. To have confidence in model predictions, the responses of the model to input parameters and the form in which the parameters are introduced must be well understood. Note that the problem with the predictions presented in Figure 13 derive from the fact that the input provided to the model did not provide a sufficiently accurate description of the pH profile. The problem is an artefact of the solver, and not of the LIRIC model itself. A comparison of LIRIC predictions with experimental data obtained in intermediate-scale studies indicates that LIRIC also models the effect of real stepwise pH changes on iodine volatility very well [3]. Intermediate-scale studies have also shown that LIRIC performs well when changes in pH are calculated within the model (as a result of organic radiolysis, for example), rather than imposed externally [3].

3.2 General Observations

The agreement between code predictions for various cases ranges from excellent to poor. For example, a plot of the predicted concentration of iodine in the gas phase for the boundary conditions corresponding to Case 1A, pH 5 (1×10^{-5} mol·dm^{-3} CsI at 90°C, irradiated at a dose rate of 1 kGy·h^{-1} and in the absence of condensing steam) are shown in Figure 14. The code predictions in the figure (with the exception of IMPAIR predictions including iodate) are very similar, with the calculated gaseous iodine fraction varying less than an order of magnitude from code to code. In contrast, Figure 15 shows case 8A, pH 5, in which the conditions are identical to Case 1A, pH 5, with the exception that there is 1×10^{-3} mol·dm^{-3} organic impurities initially in

the aqueous phase. For this case, the code predictions of the gaseous iodine inventory vary by almost three orders of magnitude.

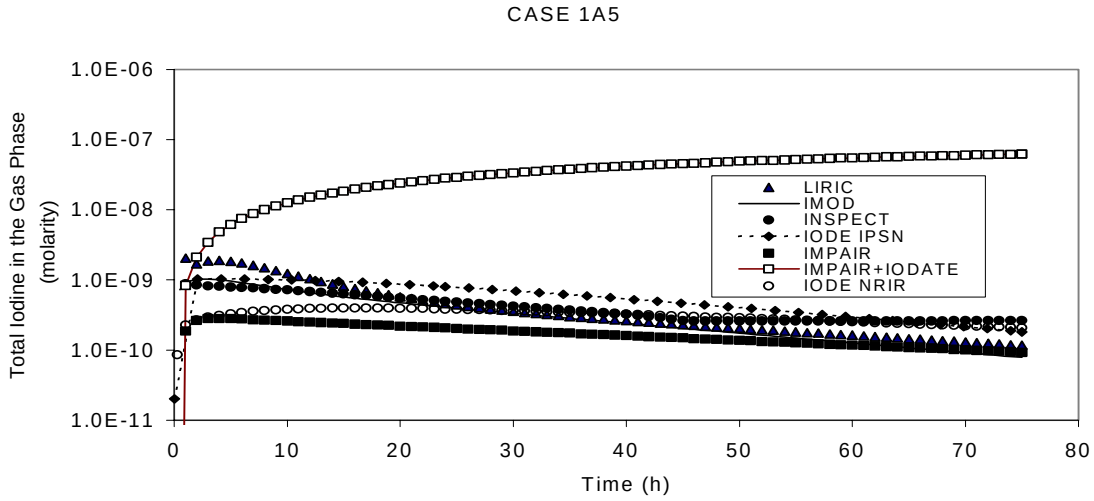

Figure 14. The total iodine concentration in the gas phase from an irradiated (1 kGy·h^{-1}) solution initially containing 1×10^{-5} mol·dm^{-3} CsI at pH 5 and at 90ºC, as predicted by the iodine behaviour codes. The sump water was assumed to be in contact with painted surfaces.

The extent to which the code predictions agree with one another varies from case to case; however, it appears that the worst agreement occurs at high dose rates, high temperature (130°C), high iodide concentration, and in the presence of large quantities of organic impurities.

In general, IMPAIR predicts a smaller gas-phase fraction than the other codes. The low values predicted by IMPAIR for the fraction of iodine in the gas phase is the result of molecular iodine being depleted in the gas phase by its reaction with O_3 to produce iodate. This extra decomposition path contributes to smaller I_2 concentrations in the gas and aqueous phase. Note, in Figure 14, that the gas-phase concentration, if IO_3^- is considered, is almost three orders of magnitude larger than if only I_2 and CH_3I are considered.

One of the most noticeable differences between the code calculations for every case is the fraction of iodine in the gas phase in the form of organic iodides. The organic iodide formation models in each code are quite different (with various dose rate, iodide and temperature dependences), and this fact is largely responsible for discrepancies between predictions of the overall gaseous iodine fractions, such as those observed in Figure 16. The organic iodide fraction at 75 h for case 1A, in which the iodide concentration was 1×10^{-5} mol·dm^{-3}, the temperature was 90°C and the dose rate was 1 kGy·h^{-1}, are shown in Table 1. Figure 16 shows a comparison of the amount of organic iodides in the gas phase as a function of time, under the same conditions as the calculations shown in Figure 14.

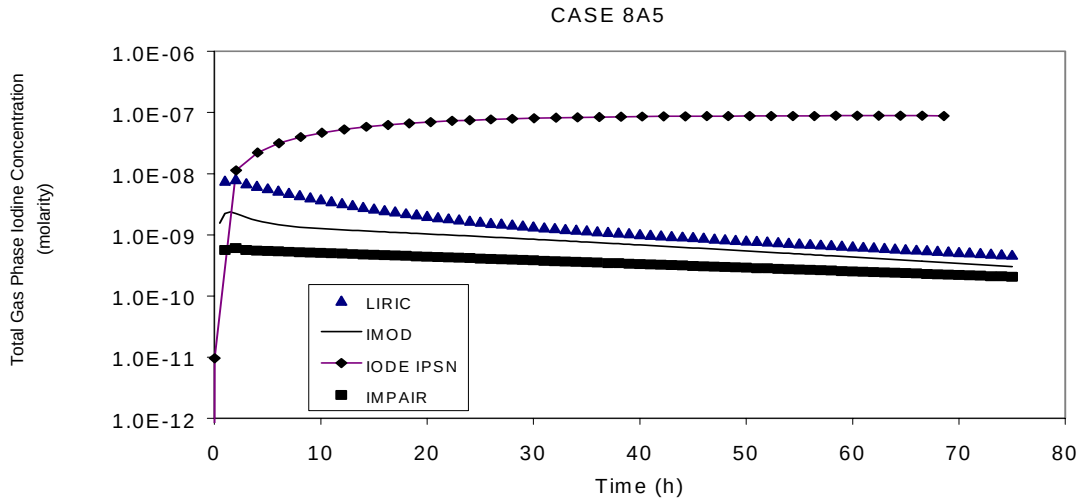

Figure 15. The total iodine concentration in the gas phase from an irradiated (1 kGy·h^{-1}) solution initially containing 1×10^{-5} mol·dm^{-3} CsI at pH 5 and at 90ºC, as predicted by the iodine behaviour codes. Organic impurities initially in the sump are assumed to be 1×10^{-3} mol·dm^{-3}.

A comparison of Figures 14 and 16 demonstrates that even when the iodine behaviour codes give very good quantitative agreement regarding the total amount of iodine in the gas phase, the percentage of the total iodine inventory in the form of gaseous organic iodides differs considerably. The variation in the amount of organic iodide predicted to be in the gas phase is also demonstrated by Table 1. The predicted percentages of organic iodides for Case 1A pH5 vary by two orders of magnitude between the codes.

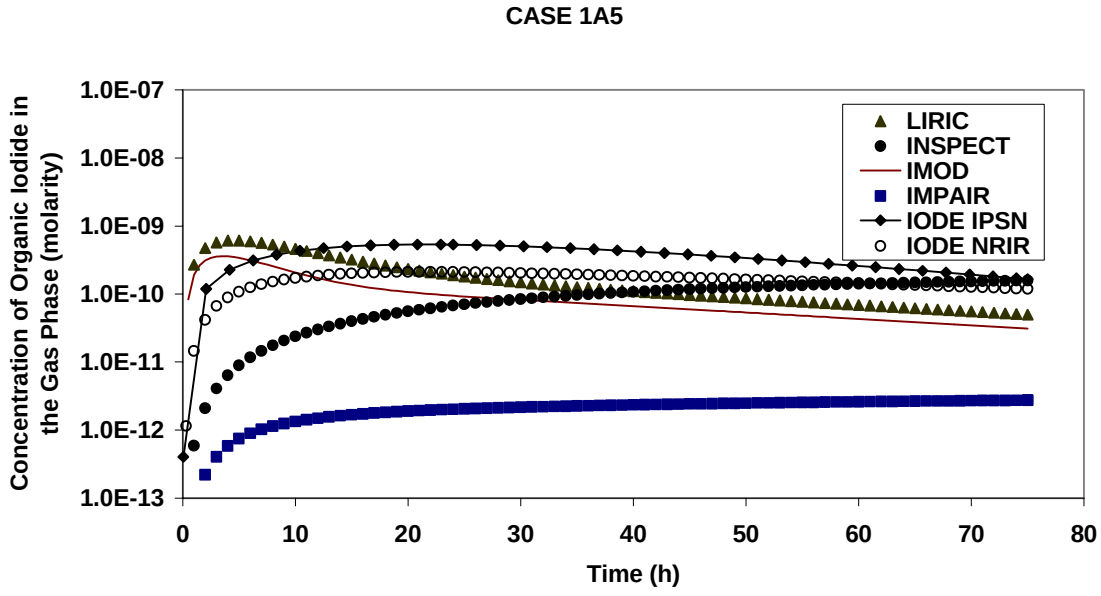

Figure 16. The organic iodide concentration in the gas phase from an irradiated ($1 kGy \cdot h^{-1}$) solution initially containing 1×10^{-5} $mol \cdot dm^{-3}$ CsI at pH 5 and at 90ºC, as predicted by the iodine behaviour codes. The sump water was assumed to be in contact with painted surfaces.

Table 1. Predicted percentage of the total iodine inventory in the form of gaseous organic iodides in case 1A at 75 h.

pH	LIRIC	IMOD	INSPECT	IODE IPSN	IODE NRIR	IMPAIR
9	1.6×10^{-3}	3.9×10^{-4}	1.8×10^{-2}	9×10^{-2}	2.2×10^{-4}	5.3×10^{-3}
5	2.4×10^{-2}	1.5×10^{-2}	1.1×10^{-1}	8.2×10^{-2}	1.2×10^{-1}	1.3×10^{-3}

4. SUMMARY

The first phase of the ISP 41 follow-up exercise, reported in this document, examined the sensitivity of iodine code predictions to a wide range of conditions anticipated in containment, with the conclusion that the codes agree reasonably well regarding the qualitative effects of most parameters on iodine volatility. The codes show similar quantitative trends under some conditions. For example, all of the codes predict that iodine volatility will decrease with increasing temperature by about the same amount, and that the gaseous iodine fraction will be rather insensitive to initial iodide concentration.

The codes all predict the same overall effect of pH, Ag and organic impurity concentrations on iodine volatility; all predict large decreases in gaseous iodide with a decrease in pH, and in the presence of silver. Most of the codes also predict that an increase in organic impurity concentration will lead to an increase in iodine volatility. However, the sensitivity of the predicted iodine volatility to these parameters varies widely from code to code. For example, with a pH change from 9 to 5, IODE(NRIR) and IMPAIR predict that iodine volatility will increase by a factor of 500,, LIRIC and IMOD predict a 50-fold increase, and IODE(IPSN) and INSPECT predict a 5- to 10-fold increase.

One significant difference in the qualitative predictions of the iodine behaviour codes is the effect of dose rate on iodine volatility. Although the reason for this discrepancy between codes is not completely clear, it is suspected that it is due to the formulation of the organic iodide formation and depletion processes. The strong dependence of iodine volatility on dose rate in many codes may be due to the fact that these codes do not model radiolytic destruction of organic iodides in this model. The dose rate dependence of organic iodide formation also varies significantly from model to model.

Under certain conditions, the quantitative agreement between code predictions is poor. In general, the agreement between code predictions was the worst at high pH values, high temperature, high dose rate, and high iodide concentrations. Agreement between the codes was also poor when the effect of organic impurities in the aqueous phase was considered. It appears that part of the reason for the wide divergence in the codes regarding the gaseous iodine fraction is also due to the way in which organic iodide formation is modelled.

5. CONCLUSIONS AND RECOMMENDATIONS

The main objective of ISP exercises is to increase confidence in the validity and accuracy of the tools that are used in assessing the safety of nuclear installations. The secondary objective is to enable code users to gain experience and demonstrate their competence. Due to the complexity of iodine behaviour in containment, the ISP 41 exercise on iodine requires three steps, in order to achieve these objectives. These steps are

1. ISP 41: Computer code exercise based on a simple RTF experiment on iodine behaviour in containment under severe accident conditions.
2. ISP 41 Follow-up Phase 1: Parametric calculations.
3. ISP 41 Follow-up Phase 2: Computer code exercise based on complex experiments performed at the RTF and Caiman facilities.

We have completed the first two steps, and recommend completing the final step.

The first step of the ISP 41 exercise demonstrated that all of the iodine behaviour codes had the capability of reproducing experimental results obtained from the RTF. However, the first step also demonstrated that the performance of these codes is extremely reliant upon the judicious choice of user-defined kinetic parameters, many of which have been chosen to provide a best fit of the code output to experimental data obtained under a narrow range of conditions (e.g., temperature, dose rate, iodide concentration, etc.). The conclusion of the exercise was that, in order to use code calculations as predictive or interpretive tools, it must be demonstrated that the kinetic parameters used in the codes are applicable to the entire range of conditions anticipated in post-accident containment.

The second step (the work reported in this document) was the first opportunity for iodine behaviour code users to assess their codes over a wide range of accident conditions. The comparison exercise allowed the code users to develop an understanding of the sensitivity of the code output to input parameters, i.e., the manner in which the predictions change as a function of each of these parameters. The parametric exercise identified several areas of discrepancy between the various codes. Most of the discrepancies appear to be quantitative in nature, i.e., the codes agree regarding the trends, but the actual amount of volatile iodine predicted by each of the codes varies considerably. The largest source of the discrepancies between code predictions appears to be the different sub-models in each code for the formation and destruction of organic iodides.

Although the current ISP exercise identified the organic iodide sub-model as contributing significantly to the discrepancy between the code predictions, parametric calculations cannot tell us which (if any) of the sub-models are correct, and what the range of user-defined input parameters for each of the sub-models could be. Therefore, we recommend that the final step of ISP 41 be a code comparison against four intermediate scale studies—two Caiman facility experiments and two RTF experiments—which examine iodine volatility over a very large range

of experimental conditions (dose rate, painted surface area, temperature, pH, etc.). In each experiment, organic iodides contributed significantly to the volatile iodine fraction.

It is recommended that the calculations first be performed as blind calculations (i.e., each code is used with default parameters). Subsequently, the results can be made available to each of the participants, and a second set of calculations can be performed, with the organic iodide models in each code being optimized (i.e., user-defined parameters being tuned to give a best fit to all of the experiments), or modified (i.e., mechanisms, or relative contributions of individual mechanisms being changed). This comparison will allow each of the code users to realistically evaluate and improve the organic iodide behaviour sub-models within each of their codes. At the least, the exercise will provide code users with optimum values for the user-defined input parameters in their iodine behaviour codes. At best, the exercise may provide insight into the organic iodide formation and destruction mechanisms themselves, and clearly identify if future experiments or changes in modelling strategy are required.

6. REFERENCES

1. J. Ball, G. Glowa, J. Wren, A.Rydl, C. Poletiko, Y. Billarand, F. Ewig, F. Funke, A. Hidaka, R. Gauntt, R. Cripps, B. Herrero and J. Royen. 2000. ISP 41 Containment Iodine Computer Code Exercise Based on a Radioiodine Test Facility (RTF) Experiment. NEA/CSNI Report, R(2000)6/ Volume 1.

2. F. Funke. 1999. Data Analysis and Modelling of Organic Iodide Production at Painted Surfaces. **In** Proceedings of OECD Workshop on Iodine Aspects of Severe Accident Management, Vantaa, Finland, 1999 May 18-20, NEA/CSNI/R (99)7, Committee on the Safety of Nuclear Installations/Organization for Economic Cooperation and Development, 151.

3. J.C. Wren and J.M Ball. 2001. LIRIC 3.2 An Updated Model for Iodine Behaviour in the Presence of Organic Impurities. Rad. Phys. Chem. **60**, 577.

APPENDIX A

ASSUMPTIONS AND BOUNDARY CONDITIONS

The following list provides the boundary conditions, initial conditions, containment geometry and other assumptions that were used for the parametric studies.

A1. Containment Geometry

Total volume = 50,000 m^3
Volume of sump water = 1,000 m^3
Liquid-gas interfacial area = 1,000 m^2
Surfaces in contact with sump water = 1,000 m^2
Surfaces in contact with the gas phase = 25,000 m^2

All surfaces are painted ⇒ Each code calculates **organic iodide formation** as a result of the presence of painted surfaces, according to its own mechanism.

All calculations were performed considering the whole containment as a single node.

A2. Initial Conditions and Input Parameters

The initial conditions and input parameters are listed in Tables 7.1 to 7.4.

A3. Output Parameters

1. Total gas-phase iodine concentration, [I(g)], as a function of time.
2. Gas-phase iodine speciation, i.e., [I_2(g)] and [org-I(g)]) as a function of time.
   (If a code allows the further separation of org-I into highly volatile and relatively nonvolatile species, then they can be presented separately. However, always provide the total organic iodide concentration.)
3. Total aqueous-phase iodine concentration, [I(aq)], as a function of time.
4. Aqueous-phase iodine speciation as a function of time:
   [I_2(aq)], [org-I(aq)] are of main interest, but others such as [IO_3^-(aq)] and [HOI(aq)], are also welcome.
5. Mass balance of iodine at the end of calculation:
   percentage of iodine inventory in the gas phase, aqueous phase and on surfaces.

A4. Duration of Calculations

Calculations were performed over a 75-h (3-day) period under a given set of conditions.

A5. Mass Transfer Coefficients

All codes essentially describe a liquid-gas interfacial mass transfer process using a two resistance model. Because of this, and to make the comparison of the results manageable, calculations were performed using same liquid-gas interfacial mass transfer coefficients:

$$\frac{1}{k_{MT}} = \frac{1}{k_{maq}} + \frac{H_{VOLI}}{k_{mg}}$$

k_{mg} (dm·s^{-1}) = 1×10^{-1} (T/298)
k_{maq} (dm·s^{-1}) = 7×10^{-3} (T/298)$^{2/3}$

where k_{MT}, k_{mg} and k_{maq} are the overall interfacial, gas-phase and aqueous-phase mass transfer coefficients, respectively, T is temperature in units of K, and H_{VOLI} is the partition coefficient of iodine species VOLI (i.e., I_2 or organic iodides)—see below.

A6. Partition Coefficients

The following partition coefficients were recommended for I_2, and for high volatile organic iodides (HVRI) and low volatile organic iodides (LVRI:

For I_2:	$\ln (H_{I2})_T = \ln 79 + (- 3600) \times (1/298 - 1/T)$
For HVRI (or CH_3I):	$\ln (H_{HVRI})_T = \ln (4) + (- 3400) \times (1/298 - 1/T)$
For LVRI:	$\ln (H_{LVRI})_T = \ln (1000) + (- 6500) \times (1/298 - 1/T)$[8]

where T is temperature (K), and $(H_x)_T$ is the partition coefficient of species x at temperature T; the partition coefficient is defined as the ratio of the aqueous-phase to the gas-phase concentration at equilibrium.

Note that these are only recommended values. Because each code handles organic iodide behaviour differently, the partition coefficients were not fixed for this exercise.

A7. Iodine Adsorption

<u>On Surfaces exposed to the gas phase</u>

---

[8] J.C. Wren and G.A. Glowa. Iodine Behaviour Models on Organic Reactions: Partitioning and Hydrolysis/Radiolysis of Organic Iodides,0 (is this "0" correct?). EPRI ACEX Report.
Please contact Jason Chao at EPRI for the report (CHAOJ@epri.com).

The iodine adsorption on dry surfaces (i.e., non-condensing conditions) in contact with the gas phase is described as a first-order process in all models. Calculations were performed using the same deposition velocities for I_2(g) on dry surfaces:

$$\ln (V_{I2})_T \text{ (dm·s}^{-1}) = \ln (1 \times 10^{-3}) + 5100 \times (1/298 - 1/T)$$

where $(V_{I2})_T$ is the deposition velocity of I_2 at temperature T in units of dm·s^{-1}. This equation gives the iodine deposition velocities:

1×10^{-3} dm·s^{-1} at 25°C,
2×10^{-2} dm·s^{-1} at 90°C, and
3×10^{-2} dm·s^{-1} at 100°C.

On Surfaces exposed to the aqueous phase

For painted surfaces contacting the sump aqueous phase, the values used for the adsorption of I_2 onto (k_{AD}) and the desorption of I_2 from (k_{DES}) were

$$k_{AD} \text{ (s}^{-1}) = v_{Paq} \cdot (A_{aq}/V_{aq})$$
$$k_{DES} \text{ (s}^{-1}) = 0$$
$$\ln\left(v_{Paq}\right) = \ln\left(v_{Paq(298K)}\right) + \left(\frac{\Delta E_{vPaq}}{R}\right) \cdot \left(\frac{1}{298} - \frac{1}{T}\right)$$
$$\Delta E_{vPaq}/R = 4900 \text{ (K)}$$
$$v_{Paq(298K)} \text{ (dm·s}^{-1}) = 0.5\times10^{-3}$$

where v_{Paq} is the deposition velocity of I_2(aq) on the surface in contact with the aqueous phase, and A_{aq} is the area of the painted surface in contact with the bulk water phase.

A8. Condensing Conditions

For condensing conditions, all walls were assumed to be covered with condensing water films, and the condensing flow rate, F_{CON}, of 1 dm^3·s^{-1} will be used for the calculations:

F_{CON} = 1.0 dm^3·s^{-1}
Thickness of the water film = 5×10^{-4} m
V_{CON} = 12.5 m^3

where V_{CON} is the total volume of condensate.

A9. pH Profile for Case 4

For the set of calculations (see Case 4 in the tables) for which pH varies with time, the following pH profile was used:

$$pH = - 3 \ln ((t + 1)^{½}) + 10$$

where t is time in **hours**.

This equation provides the pH profile shown in Figure A1.

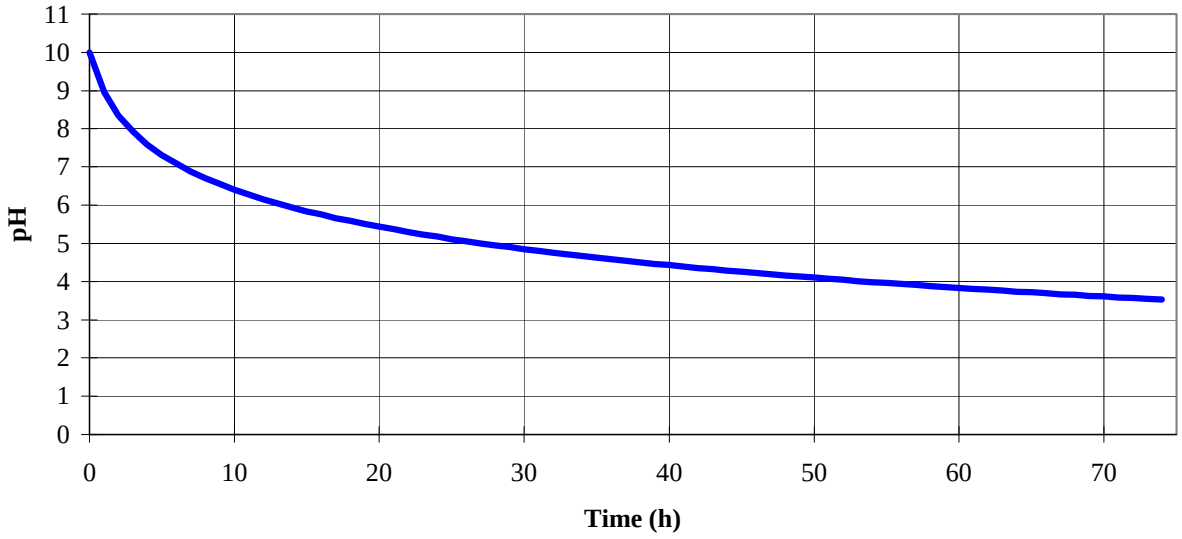

Figure A1. pH profile to be used for the calculations under case 4 conditions.

TABLES

CONDITIONS USED FOR THE PARAMETRIC STUDIES

TABLE A.1. No silver, non-condensing (i.e., no wet surfaces, except those in contact with the sump water).

Case #	Temperature (^oC)	pH	Initial $[I^-]_o$ ($mol \cdot dm^{-3}$)	Dose rate (aq) ($kGy \cdot h^{-1}$)
Case 1: Effect of temperature, constant pH, # of sets of calculations = 12				
1A9, 1A7, 1A5, 1A4	90	9,7,5,4	1×10^{-5}	1
1B9, 1B7, 1B5, 1B4	130	9,7,5,4	1×10^{-5}	1
1C9, 1C7, 1C5, 1C4	60	9,7,5,4	1×10^{-5}	1
Case 2: Effect of initial $[I^-]_o$, constant pH, # of sets of calculations = 8				
2A9, 2A7, 2A5, 2A4	90	9,7,5,4	1×10^{-6}	1
2B9, 2B7, 2B5, 2B4	90	9,7,5,4	1×10^{-4}	1
Case 3: Effect of dose rate (aq), constant pH, # of sets of calculations = 8				
3A9, 3A7, 3A5, 3A4	90	9,7,5,4	1×10^{-5}	10
3B9, 3B7, 3B5, 3B4	90	9,7,5,4	1×10^{-5}	0.1
Case 4: Varying pH, # of sets of calculations = 3 $pH = 3 \ln ((t + 1)^{½}) + 10$, t in hours				
4A	90	varying with t	1×10^{-5}	1
4B	90	varying with t	1×10^{-4}	1
4C	90	varying with t	1×10^{-6}	1
Case 5[a]: Uncontrolled pH, starting pH = 10, # of sets of calculations = 3 Comparison of different acid formation mechanisms used in various codes.				
5A	90	uncontrolled	1×10^{-5}	1
5B	90	uncontrolled	1×10^{-5}	10
5C	60	uncontrolled	1×10^{-5}	1

[a]Case 5 is not required for codes for which pH is an input parameter. (continued)

TABLE A.2. No silver, condensing (condensate volume = 12,500 dm^3, volume flow rate = 1 dm^3/s, condensing film thickness = 5×10^{-3} dm).

Case 6: Effect of condensation, constant pH, # of sets of calculations = 8				
Case #	Temperature (^oC)	pH	Initial $[I^-]_o$ ($mol\cdot dm^{-3}$)	Dose rate (aq) ($kGy\cdot h^{-1}$)
6A9, 6A7, 6A5, 6A4	90	9,7,5,4	1×10^{-5}	1
6B9, 6B7, 6B5, 6B4	130	9,7,5,4	1×10^{-5}	1

TABLE A.3: Non-condensing, silver present (amount of Ag = 100 kg in the sump water, surface area of Ag = 800 m^2/kg Ag, 10% of Ag is present as AgO_x for a code which requires oxidized silver).

Case 7: Effect of silver, constant pH, # of sets of calculations = 8				
Case #	Temperature (^oC)	pH	Initial $[I^-]_o$ ($mol\cdot dm^{-3}$)	Dose rate (aq) ($kGy\cdot h^{-1}$)
7A9, 7A7, 7A5, 7A4	90	9,7,5,4	1×10^{-4}	1
7B9, 7B7, 7B5, 7B4	90	9,7,5,4	1×10^{-5}	1

TABLE A.4. No silver, non-condensing, organic impurities initially present in the sump.

(For these calculations, no other sources of organic impurities in the sump water, such as the dissolution of solvents from painted surfaces, or no organic iodide formation other than via reactions with the initially present organic impurities, would be considered.)

Case 8: Constant pH, # of sets of calculations = 12 Effect of organic impurities in the sump: for A & B, $[Org]_o = 1\times10^{-3}$ $mol\cdot dm^{-3}$; for C, $[Org]_o = 1\times10^{-5}$ $mol\cdot dm^{-3}$.				
Case #	Temperature (^oC)	pH	Initial $[I^-]_o$ ($mol\cdot dm^{-3}$)	Dose rate (aq) ($kGy\cdot h^{-1}$)
8A9, 8A7, 8A5, 8A4	90	9,7,5,4	1×10^{-5}	1
8B9, 8B7, 8B5, 8B4	130	9,7,5,4	1×10^{-5}	1
8C9, 8C7, 8C5, 8C4	90	9,7,5,4	1×10^{-5}	1

APPENDIX B

SELECTED MASS BALANCES AT 75 h[9]

Case 1A pH 9, 90 °C, 10^{-5} M I^-, 1kGy/h	% Gas	% Aqueous	% Surface (g)	% Surface (aq)
IMOD	3.9E-03	9.7E+01	1.1	2.0
LIRIC	2.1E-03	9.9E+01	1.4E-01	1.0
IMPAIR	2.2E-02	9.8E+01	3.0E-02	1.6
INSPECT	2.7E-02	9.8E+01	1.9	2.8E-04
IODE-IPSN	9.0E-02	1.0E+02	1.0E-02	3.0E-02
IODE NRIR	7.4E-04	1.0E+02	data not available	data not available

Case 1A pH 5, 90 °C, 10^{-5} M I^- 1kGy/h	% Gas	% Aqueous	% Surface (g)	% Surface (aq)
IMOD	3.8E-02	5.5	3.4E+01	6.0E+01
LIRIC	2.5E-02	1.5	1.2E+01	8.6E+01
IMPAIR	2.9E+01	3.0E+01	4.0E+01	5.9E-01
INSPECT	1.28E-01	5.3	3.1E+01	6.3E+01
IODE-IPSN	9.0E-02	1.8	3.2E+01	6.6E+01
IODE NRIR	1.0E-01	3.8E+01	2.0E+01	4.2E+01

Case 1B pH 9, 130°C, 10^{-5} M I^- 1kGy/h	% Gas	% Aqueous	% Surface (g)	% Surface (aq)
IMOD	5.9E-04	9.7E+01	5.7E-01	2.4
LIRIC	1.9E-04	9.8E+01	5.6E-02	1.5
IMPAIR	4.0E-03	9.3E+01	1.0E-02	7.5
INSPECT	3.9E-02	9.8E+01	1.8	1.8E-04
IODE-IPSN	4.0E-03	1.0E+02	3.0E-02	1.0E-02
IODE NRIR	5.0E-05	1.0E+02	data not available	data not available

[9] Note that IMPAIR gas-phase percentages include IO_3^- aerosol.

APPENDIX B. SELECTED MASS BALANCES AT 75 h[10] (continued)

Case 1B pH 5, 130°C, 10^{-5} MI^- 1kGy/h	% Gas	% Aqueous	% Surface (g)	% Surface (aq)
IMOD	6.7E-03	4.4E+01	1.1E+01	4.5E+01
LIRIC	4.2E-03	1.1E+01	6.4	8.3E+01
IMPAIR	2.5E+01	3.1E+01	4.1E+01	2.7
INSPECT	1.5E-01	1.0E+01	1.4E+01	7.6E+01
IODE-IPSN	3.0E-03	1.4	1.6E+01	8.3E+01
IODE NRIR	3.0E-02	3.75E+01	2.0E+01	4.2E+01

Case 1C pH 9, 60°C, 10^{-5} M I^- 1kGy/h	% Gas	% Aqueous	% Surface (g)	% Surface (aq)
IMOD	1.8E-02	9.7E+01	1.3E+00	1.7
LIRIC	7.0E-03	9.8E+01	4.7E-01	1.3
IMPAIR	5.3E-02	9.8E+01	4.8E-02	2.1
INSPECT	3.1E-02	9.8E+01	1.5	5.3E-04
IODE-IPSN	4.2E-01	9.9E+01	5.0E-02	6.0E-02
IODE NRIR	2.0E-02	1.0E+02	data not available	data not available

Case 1C pH 5, 60°C, 10^{-5} M I^- 1kGy/h	% Gas	% Aqueous	% Surface (g)	% Surface (aq)
IMOD	7.4E-02	5.4E-02	4.4E+01	5.6E+01
LIRIC	3.2E-02	5.4E-01	2.7E+01	7.3E+01
IMPAIR	3.6E+01	2.9E+01	3.3E+01	1.3
INSPECT	1.0E-01	2.2	4.3E+01	5.5E+01
IODE-IPSN	9.8E-01	3.7	4.1E+01	5.5E+01
IODE NRIR	1.6	4.0E+01	2.5E+01	3.3E+01

[10] Note that IMPAIR gas-phase percentages include IO_3^- aerosol.

APPENDIX B: SELECTED MASS BALANCES AT 75 h[11] (continued)

Case 2A pH 9, 90°C, 10^{-6} M I^- 1kGy/h	% Gas	% Aqueous	% Surface (g)	% Surface (aq)
IMOD	3.9E-03	9.7E+01	1.1	2.0
LIRIC	4.2E-03	1.0E+02	1.4E-02	1.0E-01
IMPAIR	1.9E-02	9.8E+01	2.5E-02	1.6
INSPECT	2.2E-01	8.3E+01	1.6E+01	1.7E-03
IODE-IPSN	9.0E-02	1.0E+02	4.0E-03	1.0E-02

Case 2A pH 5, 90°C, 10^{-6} M I^- 1kGy/h	% Gas	% Aqueous	% Surface (g)	% Surface (aq)
IMOD	3.8E-02	4.7	3.3E+01	6.2E+01
LIRIC	4.1E-02	1.0E+01	1.1E+01	7.9E+01
IMPAIR	2.9E+01	3.1E+01	3.9E+01	6.0E-01
INSPECT	2.9E-01	5.0E+01	2.4E+01	2.5E+01
IODE-IPSN	9.0E-02	3.5	3.1E+01	6.5E+01
IODE-NRIR	1.0E-01	3.8E+01	2.0E+01	4.2E+01

Case 2B pH 9, 90°C, 10^{-4} M I^- 1kGy/h	% Gas	% Aqueous	% Surface (g)	% Surface (aq)
IMOD	3.8E-03	9.7E+01	1.1	2.0
LIRIC	1.3E-03	9.7E+01	3.5E-01	2.6
IMPAIR	3.2E-02	9.8E+01	4.4E-02	1.6
INSPECT	1.0E-03	1E+02	6.9E-02	3.6E-05
IODE-IPSN	9.0E-02	1.0E+02	4.0E-02	9.0E-02
IODE-NRIR	2.5E-02	1.0E+02	data not available	data not available

[11] Note that IMPAIR gas-phase percentages include IO_3^- aerosol.

APPENDIX B: SELECTED MASS BALANCES AT 75 h[12] (continued)

Case 2B pH 5, 90°C, 10^{-4} M I^- 1kGy/h	% Gas	% Aqueous	% Surface (g)	% Surface (aq)
IMOD	1.39E-01	12.0E+01	3.6E+01	5.2E+01
LIRIC	1.9E-02	9.2E-01	7.8E+01	2.1E+01
IMPAIR	2.9E+01	3.0E+01	4.0E+01	5.9E-01
INSPECT	4.5E-02	3.0	3.1E+01	6.7E+01
IODE-IPSN	9.0E-02	1.7	3.2E+01	6.6E+01
IODE-NRIR	1.0E-01	3.8E+01	2.0E+01	4.2E+01

Case 3A pH 9, 90°C, 10^{-5} M I^- 10kGy/h	% Gas	% Aqueous	% Surface (g)	% Surface (aq)
IMOD	1.2E-03	9.1E+01	3.26	6.07
LIRIC	2.2E-03	9.9E+01	1.4E-01	1.1
IMPAIR	1.9E-02	9.8E+01	2.7E-02	1.6
INSPECT	8.5E-02	9.5E+01	5.0	6.8E-04
IODE-IPSN	8.8E-01	9.9E+01	4.0E-02	9.0E-02
IODE-NRIR	1.0E-02	1.0E+02	data not available	data not available

Case 3A pH 5, 90°C, 10^{-5} M I^- 10kGy/h	% Gas	% Aqueous	% Surface (g)	% Surface (aq)
IMOD	1.4E-02	1.9e-2	6.4E+01	3.6E+01
LIRIC	4.3E-02	1.6	1.2E+01	8.6E+01
IMPAIR	4.1E+01	1.6	5.7E+01	8.0E-04
INSPECT	1.2E-01	1.9E+01	2.6E+01	5.5E+01
IODE-IPSN	5.0E-02	1.8	3.2E+01	6.6E+01
IODE-NRIR	5.4E-02	5.1E-01	3.2E+01	6.7E+01

[12] Note that IMPAIR gas-phase percentages include IO_3^- aerosol.

APPENDIX B: SELECTED MASS BALANCES AT 75 h[13] (continued)

Case 3B pH 9, 90°C, 10^{-5} M I^- 0.1kGy/h	% Gas	% Aqueous	% Surface (g)	% Surface (aq)
IMOD	1.2E-03	9.9E+01	3.4E-01	6.4E-01
LIRIC	6.8E-03	9.9E+01	1.4E-01	1.0
IMPAIR	2.3E-02	9.8E+01	2.4E-01	1.6
INSPECT	7.7E-03	9.9E+01	6.3E-01	3.8E-05
IODE-IPSN	1.0E-02	1.0E+02	0.0E+00	1.0E-02
IODE-NRIR	1.0E-04	1.0E+02	data not available	data not available

Case 3B pH 5, 90°C, 10^{-5} M I^- 0.1kGy/h	% Gas	% Aqueous	% Surface (g)	% Surface (aq)
IMOD	5.2E-03	3.9E+01	2.2E+01	3.9E+01
LIRIC	3.2E-03	1.3	1.2E+01	8.6E+01
IMPAIR	4.8	8.7E+01	6.6	1.5
INSPECT	1.2E-01	1.9E+01	2.6E+01	5.5E+01
IODE-IPSN	9.0E-02	6.6E+01	1.1E+01	2.3E+01
IODE-NRIR	1.1E-02	9.0E+01	3.1	6.4

Case 4A, 90°C,10^{-5} M I^- 1 kGy/h	% Gas	% Aqueous	% Surface (g)	% Surface (aq)
IMOD	1.5E-02	3.2E-01	3.6E+01	6.4E+01
LIRIC	9.6E-03	3.9E-01	8.7E+01	1.2E+01
IMPAIR	3.6E+01	1.3E+01	5.0E+01	4.1E-01
INSPECT	1.1E-01	8.0E+01	3.2E+01	6.7E+01
IODE-IPSN	1.1E-01	8.0E-02	3.2E+01	6.8E+01
IODE-NRIR	1.4E-01	3.7E+01	2.0E+01	4.3E+01

[13] Note that IMPAIR gas-phase percentages include IO_3^- aerosol.

APPENDIX B: SELECTED MASS BALANCES AT 75 h[14] (continued)

Case4B 90°C,10^{-4} M I⁻1 kGy/h	% Gas	% Aqueous	% Surface (g)	% Surface (aq)
IMOD	1.74E-01	1.9	4.1E+01	5.7E+01
LIRIC	1.2E-02	4.2E-01	2.1E+01	7.9E+01
IMPAIR	3.6E+01	1.3E+01	5.0E+01	4.1E-01
INSPECT	2.9E-02	8.5E-02	3.1E+01	6.9E+01
IODE-IPSN	1.1E-01	4.0E-02	3.2E+01	6.8E+01
IODE-NRIR	1.4E-01	3.6E+01	2.0E+01	4.3E+01

Case 4C 90°C,10^{-6} M I⁻1 kGy/h	% Gas	% Aqueous	% Surface (g)	% Surface (aq)
IMOD	7.7E-03	2.1E-01	3.5E+01	6.5E+01
LIRIC	1.6E-02	2.7E+00	1.2E+01	8.6E+01
IMPAIR	3.6E+01	1.3E+01	5.0E+01	4.1E-01
INSPECT	3.9E-01	7.9E+00	3.7E+01	5.5E+01
IODE-IPSN	1.2E-01	5.4E-01	3.2E+01	6.7E+01
IODE-NRIR	1.4E-01	3.7E+01	2.0E+01	4.3E+01

Case5A 90°C,10^{-5} M I⁻1 kGy/h	% Gas	% Aqueous	% Surface (g)	% Surface (aq)
IMOD	1.9E-02	8.4E+01	5.8	1.1E+01
LIRIC	9.3E-03	7.9E+01	2.5	1.9E+01
IMPAIR	No Data	No Data	No Data	No Data
INSPECT	2.0E-02	9.8E+01	1.5	2.1E-05
IODE-IPSN	2.1E-01	9.5E+01	1.6	3.3

[14] Note that IMPAIR gas-phase percentages include IO_3^- aerosol.

APPENDIX B: SELECTED MASS BALANCES AT 75 h[15] (continued)

Case5B 90°C,10^{-5} M I⁻10 kGy/h	% Gas	% Aqueous	% Surface (g)	% Surface (aq)
IMOD	4.0E-02	5.4E+01	1.6E+01	3.0E+01
LIRIC	1.1E-02	7.2E+01	3.3	2.4E+01
IMPAIR	NO Data	NO Data	NO Data	NO Data
INSPECT	6.9E-02	9.6E+01	3.7	4.4E-5
IODE-IPSN	1.7	8.4E+01	4.6	9.6

Case 5C 60°C,10^{-5} M I⁻1 kGy/h	% Gas	% Aqueous	% Surface (g)	% Surface (aq)
IMOD	1.4E-01	7.6E+01	1.0E+01	1.3E+01
LIRIC	8.7E-02	5.9E+01	1.1E+01	3.0E+01
IMPAIR	No Data	No Data	No Data	No Data
INSPECT	2.5E-02	9.9E+01	1.3E+00	5.3E-05
IODE-IPSN	9.7E-01	8.6E+01	5.4	7.3

Case 6A pH 9,90°C, 10^{-5} M I⁻ 1 kGy/h	% Gas	% Aqueous	% Surface (g)	% Surface (aq)
IMOD	1.4E-02	9.8E+01	1.4E-01	2.0
LIRIC	3.6E-02	9.9E+01	1.9E-02	1.0
IMPAIR	3.3E-02	9.8E+01	1.5E-02	1.6
INSPECT	2.3E-02	9.8E+01	1.8	2.8E-04
IODE-IPSN	4.0E-02	1.0E+02	1.0E-02	3.0E-02

[15] Note that IMPAIR gas-phase percentages include IO_3^- aerosol.

APPENDIX B: SELECTED MASS BALANCES AT 75 h[16] (continued)

Case 6A pH 5, 90°C,10^{-5} M I^- 1 kGy/h	% Gas	% Aqueous	% Surface (g)	% Surface (aq)
IMOD	4.1E-01	1.5E+01	5.9	7.8E+01
LIRIC	9.1E-02	2.0	1.8	9.6E+01
IMPAIR	4.9E+01	2.8E+01	2.2E+01	5.6E-01
INSPECT	1.0E-01	5.4	3.1E+01	6.4E+01
IODE-IPSN	1.8E-02	1.8	3.1E+01	6.7E+01
IODE-NRIR	4.4E-02	3.8E+01	8.6	5.3E+01

Case 6B pH 9, 130°C,10^{-5} M I^- 1 kGy/h	% Gas	% Aqueous	% Surface (g)	% Surface (aq)
IMOD	2.1E-03	9.7E+01	2.1E-01	2.4
LIRIC	2.1E-03	9.9E+01	2.3E-02	1.5
IMPAIR	8.7E-03	9.2E+01	1.1E-03	7.5
INSPECT	3.0E-02	9.8E+01	1.8	2.8E-04
IODE-IPSN	2.0E-03	1.0E+02	3.0E-03	1.4E-02

Case 6B pH 5, 130°C,10^{-5} M I^- 1 kGy/h	% Gas	% Aqueous	% Surface (g)	% Surface (aq)
IMOD	3.2E-02	4.9E+01	4.3	4.7E+01
LIRIC	5.5E-03	2.8	1.6	9.6E+01
IMPAIR	5.8E+01	3.3E+01	6.1E+00	2.8
INSPECT	1.1E-01	1.2E+01	1.4E+01	7.6E+01
IODE-IPSN	1.1E-03	1.4	1.6E+01	8.3E+01
IODE-NRIR	2.9E-02	3.8E+01	1.0E+01	5.2E+01

[16] Note that IMPAIR gas-phase percentages include IO_3^- aerosol.

APPENDIX B: SELECTED MASS BALANCES AT 75 h[17] (continued)

Case 7A pH 9, 90°C,10^{-4} M I^- 1 kGy/h	% Gas	% Aqueous	% Surface (g)	% Surface (aq)
IMOD	8.8E-04	2.1E+01	5.5E-01	1.0
LIRIC	2.8E-04	1.5E+01	1.5E-01	1.3
IMPAIR	3.1E-02	9.4E+01	4.0E-02	1.6
INSPECT	2.5E-04	1.5E-03	1.6E-02	5.3E-07
IODE-IPSN	6.8E-04	7.3E-01	4.8E-03	1.0E-02

Case 7A pH 5, 90°C, 10^{-4} M I^- 1 kGy/h	% Gas	% Aqueous	% Surface (g)	% Surface (aq)
IMOD	4.6E-04	1.4E-03	6.9E-01	1.3
LIRIC	1.3E-04	1.1E-04	1.8E-01	1.5
IMPAIR	2.9E+01	2.8E+01	4.0E+01	5.6E-01
INSPECT	1.1E-03	1.7E-02	7.1E-04	6.6E-02
IODE-IPSN	Missing Data	Missing Data	Missing Data	Missing Data

Case 7B pH 9, 90°C,10^{-5} M I^- 1 kGy/h	% Gas	% Aqueous	% Surface (g)	% Surface (aq)
IMOD	1.1E-04	2.3E+01	5.6E-02	1.0E-01
LIRIC	1.6E-03	5.5E+01	7.8E-02	6.9E-01
IMPAIR	2.2E-02	9.8E+01	2.9E-02	1.6
INSPECT	2.2E-03	1.5E-02	1.3E-01	1.4E-06
IODE-IPSN	9.1E-07	1.0E-06	2.4E-10	5.1E-10

[17] Note that IMPAIR gas-phase percentages include IO_3^- aerosol.

APPENDIX B: SELECTED MASS BALANCES AT 75 h[18] (continued)

Case 7B pH 5, 90°C,10^{-5}M I^- 1 kGy/h	% Gas	% Aqueous	% Surface (g)	% Surface (aq)
IMOD	1.6E-04	2.8E-06	7.4E-02	1.4E-01
LIRIC	4.4E-04	7.9E-04	1.7E-01	1.3
IMPAIR	2.9E+01	3.1E+01	4.0E+01	5.6E-01
INSPECT	5.6E-03	1.6E-01	3.5E-01	4.1E-02
IODE-IPSN	8.3E-06	1.1E-04	1.4E-04	2.9E-04

Case 8A pH 9, 90°C,10^{-5}M I^-1 kGy/h 10^{-3} M RH	% Gas	% Aqueous	% Surface (g)	% Surface (aq)
IMOD	8.5E-03	9.7E+01	1.1	2.0
LIRIC	2.2E-02	9.9E+01	1.4E-01	1.0
IMPAIR	4.9E-02	9.8E+01	6.6E-02	1.6
INSPECT	No Data	No Data	No Data	No Data
IODE-IPSN	2.3E-01	1.0E+02	1.0E-02	3.0E-02

Case 8A pH 5, 90°C,10^{-5} M I^- 1 kGy/h 10^{-3} M RH	% Gas	% Aqueous	% Surface (g)	% Surface (aq)
IMOD	1.5E-01	5.6	3.4E+01	6.0E+01
LIRIC	2.3E-01	1.7	8.6E+01	1.2E+01
IMPAIR	2.7E+01	3.5E+01	3.7E+01	6.9E-01
INSPECT	No Data	No Data	No Data	No Data
IODE-IPSN	4.3E+01	4.9E+01	2.7	5.7

[18] Note that IMPAIR gas-phase percentages include IO_3^- aerosol.

APPENDIX B: SELECTED MASS BALANCES AT 75 h[19] (continued)

Case 8B pH 9, 130°C,10^{-5} M I^- 1 kGy/h 10^{-3} M RH	% Gas	% Aqueous	% Surface (g)	% Surface (aq)
IMOD	6.0E-04	9.7E+01	5.7E-01	2.4
LIRIC	1.3E-03	9.3E+01	6.6	6.5E-02
IMPAIR	1.6E-03	9.2E+01	2.7E-03	7.6
INSPECT	No Data	No Data	No Data	No Data
IODE-IPSN	3.0E-03	1.0E+02	3.0E-03	1.4E-02

Case 8B pH 5, 130°C,10^{-5} M I^- 1 kGy/h 10^{-3} M RH	% Gas	% Aqueous	% Surface (g)	% Surface (aq)
IMOD	9.5E-03	4.4E+01	1.1E+01	4.5E+01
LIRIC	8.2E-02	2.5	4.0	9.3E+01
IMPAIR	2.0E+01	4.2E+01	3.4E+01	3.7
INSPECT	No Data	No Data	No Data	No Data
IODE-IPSN	2.8	7.8E+01	3.1	1.6E+01

Case 8C pH 9, 90°C,10^{-5} M I^- 1 kGy/h 10^{-5} M RH	% Gas	% Aqueous	% Surface (g)	% Surface (aq)
IMOD	3.6E-03	9.7E+01	1.1	2.0
LIRIC	6.7E-04	9.9E+01	1.4E-01	1.0
IMPAIR	4.9E-03	9.8E+01	6.8E-03	1.6
INSPECT	No Data	No Data	No Data	No Data
IODE-IPSN	3.0E-03	1.0E+02	1.0E-02	3.0E-02

[19] Note that IMPAIR gas-phase percentages include IO_3^- aerosol.

APPENDIX B: SELECTED MASS BALANCES AT 75 h[20] (concluded)

Case 8C pH 5, 90°C, 10^{-5} M I^- 1 kGy/h 10^{-5} M RH	% Gas	% Aqueous	% Surface (g)	% Surface (aq)
IMOD	2.6E-02	7.4E+01	9.3	1.7E+01
LIRIC	8.2E-02	2.5	4.0	9.3E+01
IMPAIR	2.9E+01	3.0E+01	4.0E+01	6.0E-01
INSPECT	No Data	No Data	No Data	No Data
IODE-IPSN	2.3	4.7	3.0E+01	6.3E+01
IODE-NRIR	4.4E-02	3.7E+01	2.0E+01	4.3E+01

[20] Note that IMPAIR gas-phase percentages include IO_3^- aerosol.

APPENDIX C

CALCULATION RESULTS

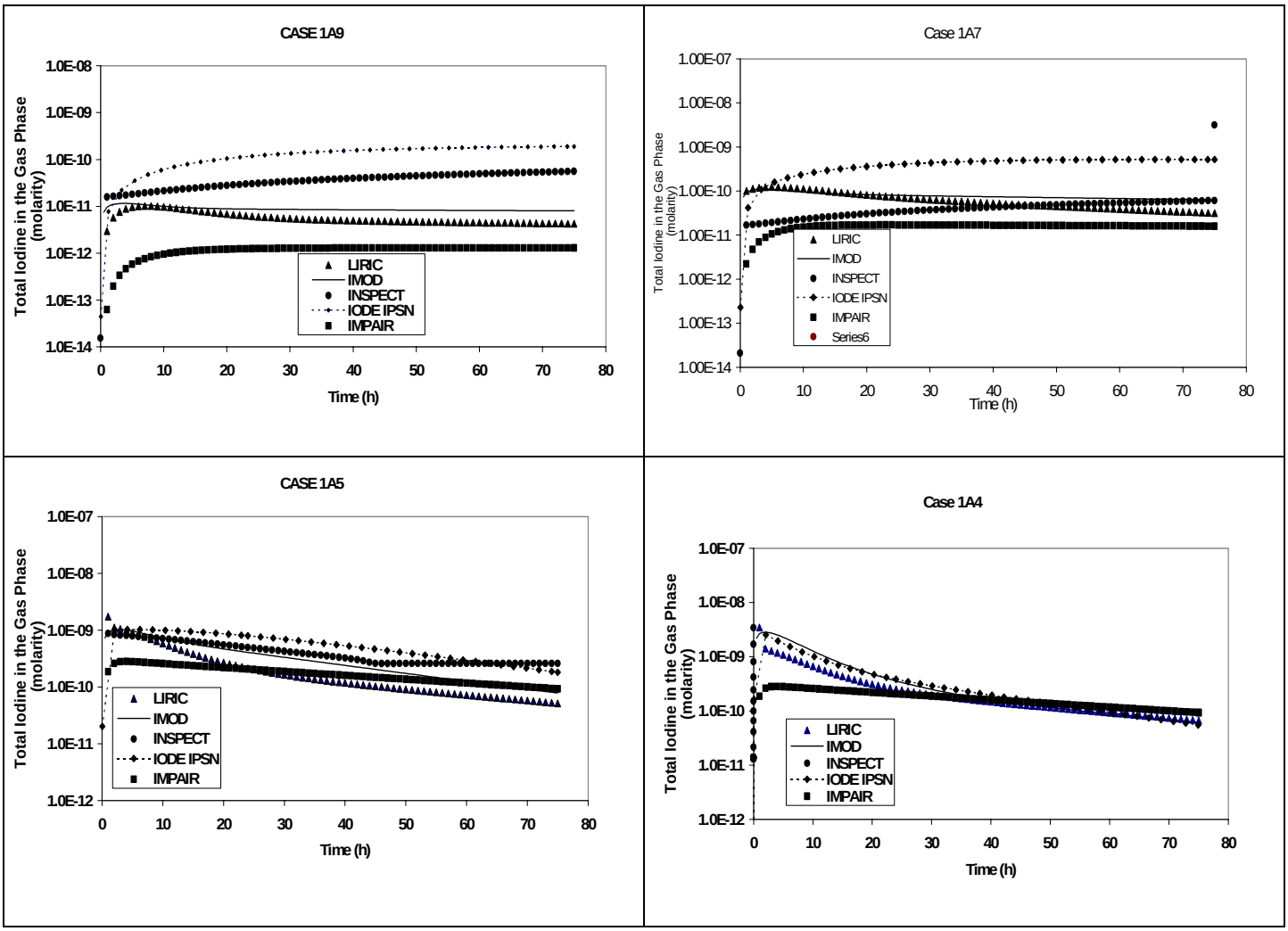

Case 1A. Percentage of iodine inventory in the gas phase for 1×10^{-5} mol·dm^{-3} CsI at 90°C, irradiated at a dose rate of 1 k·Gyh^{-1}. No condensation, sump water is assumed to contact painted surfaces.

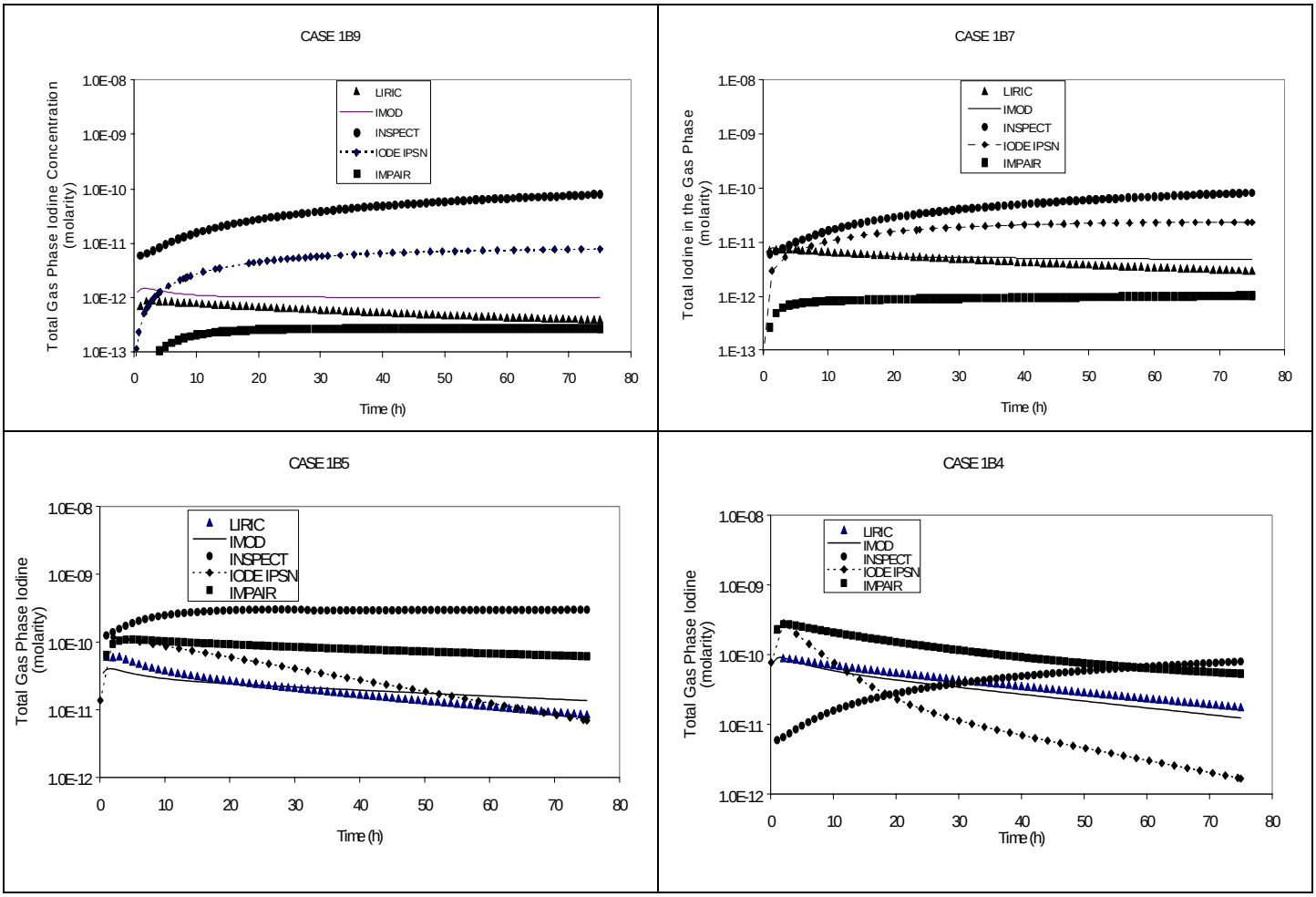

Case 1B. Percentage of iodine inventory in the gas phase for 1×10^{-5} mol·dm^{-3} CsI at 130°C, irradiated at a dose rate of 1 kGy·h^{-1}. No condensation, sump water is assumed to contact painted surfaces.

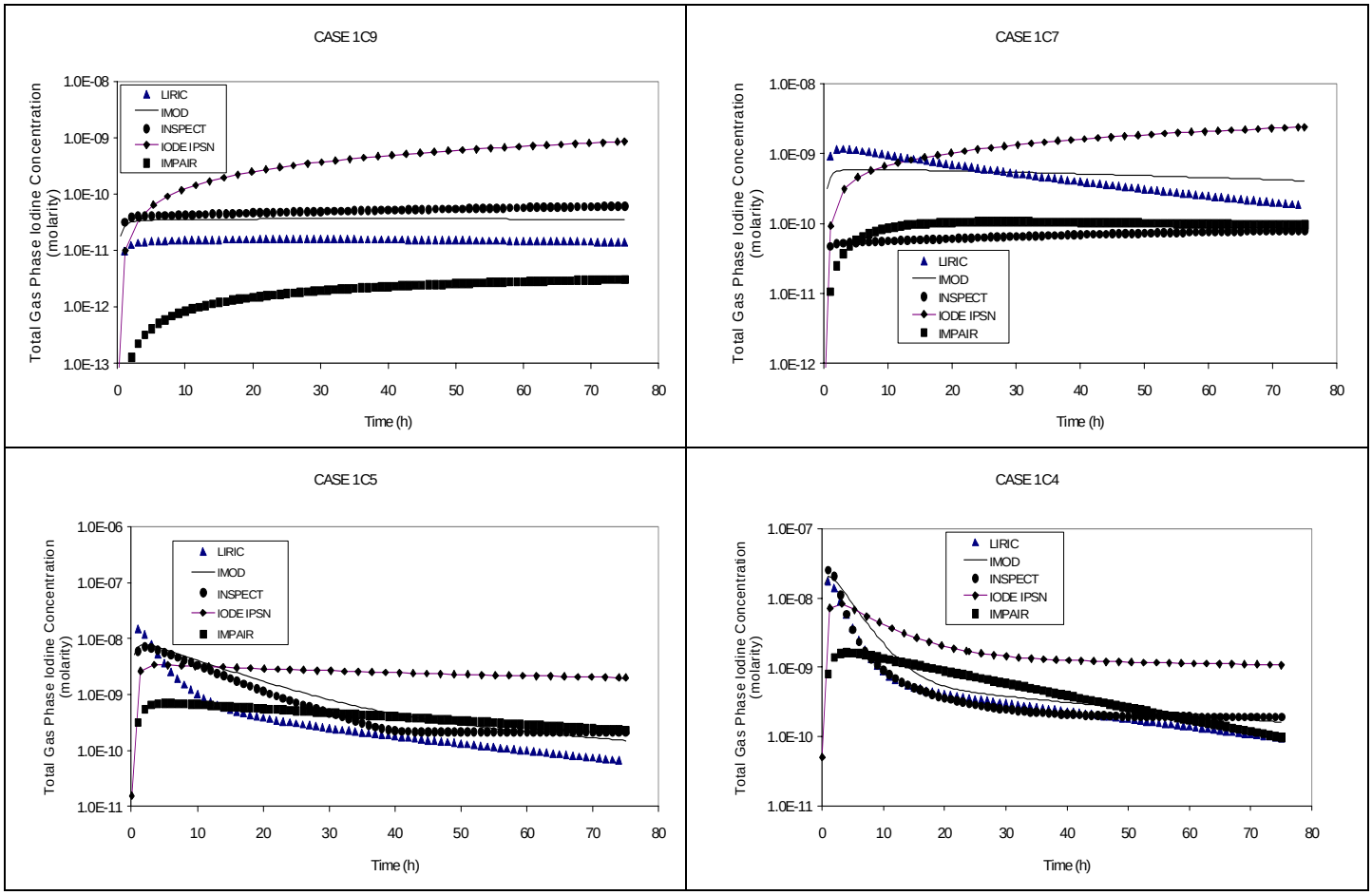

Case 1C. Percentage of iodine inventory in the gas phase for 1×10^{-5} mol·dm^{-3} CsI at 60°C, irradiated at a dose rate of 1 kGy·h^{-1}. No condensation, sump water is assumed to contact painted surfaces.

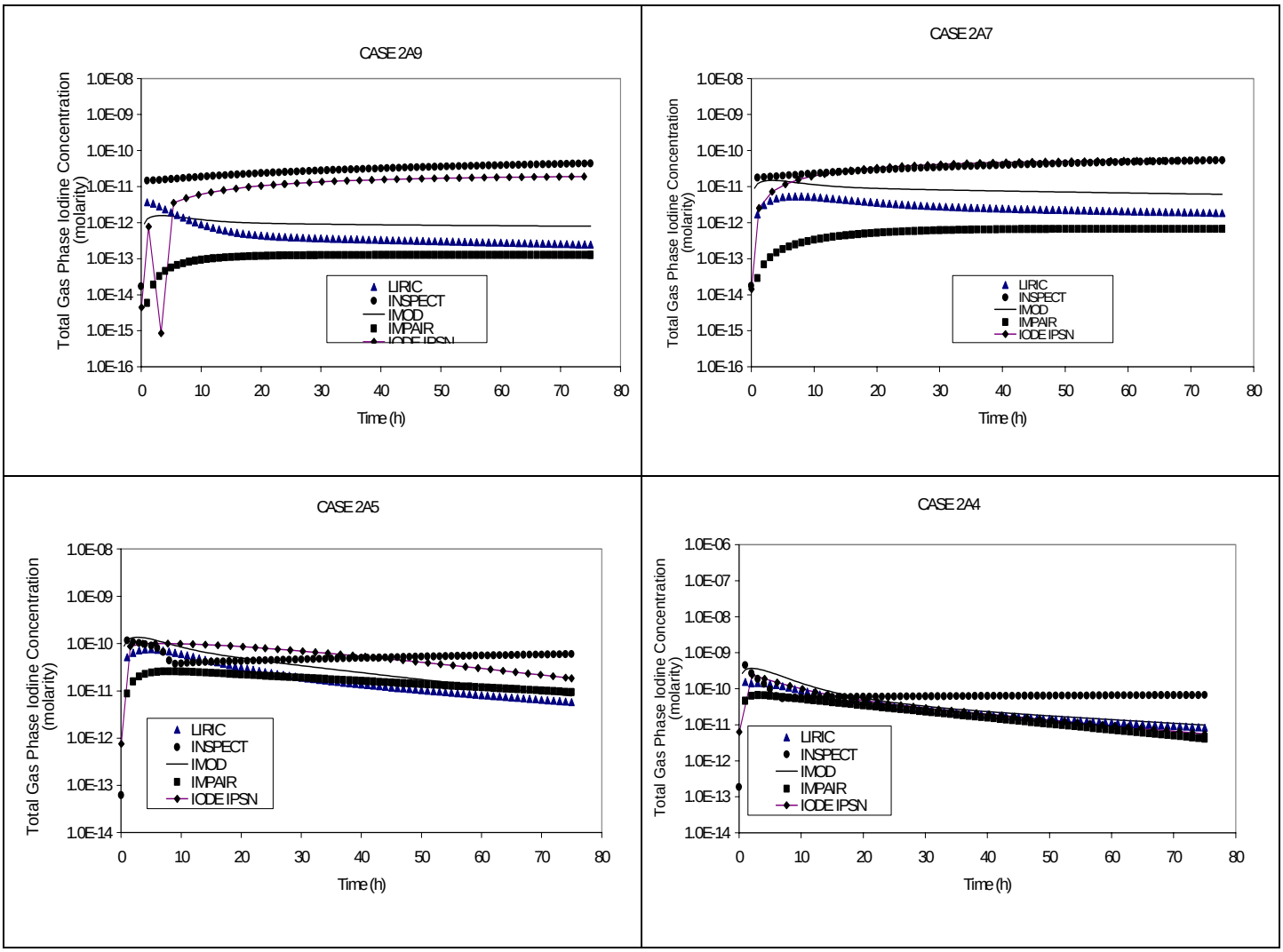

Case 2A. Percentage of iodine inventory in the gas phase for 1×10^{-6} mol·dm^{-3} CsI at 90°C, irradiated at a dose rate of 1 kGy·h^{-1}. No condensation, sump water is assumed to contact painted surfaces.

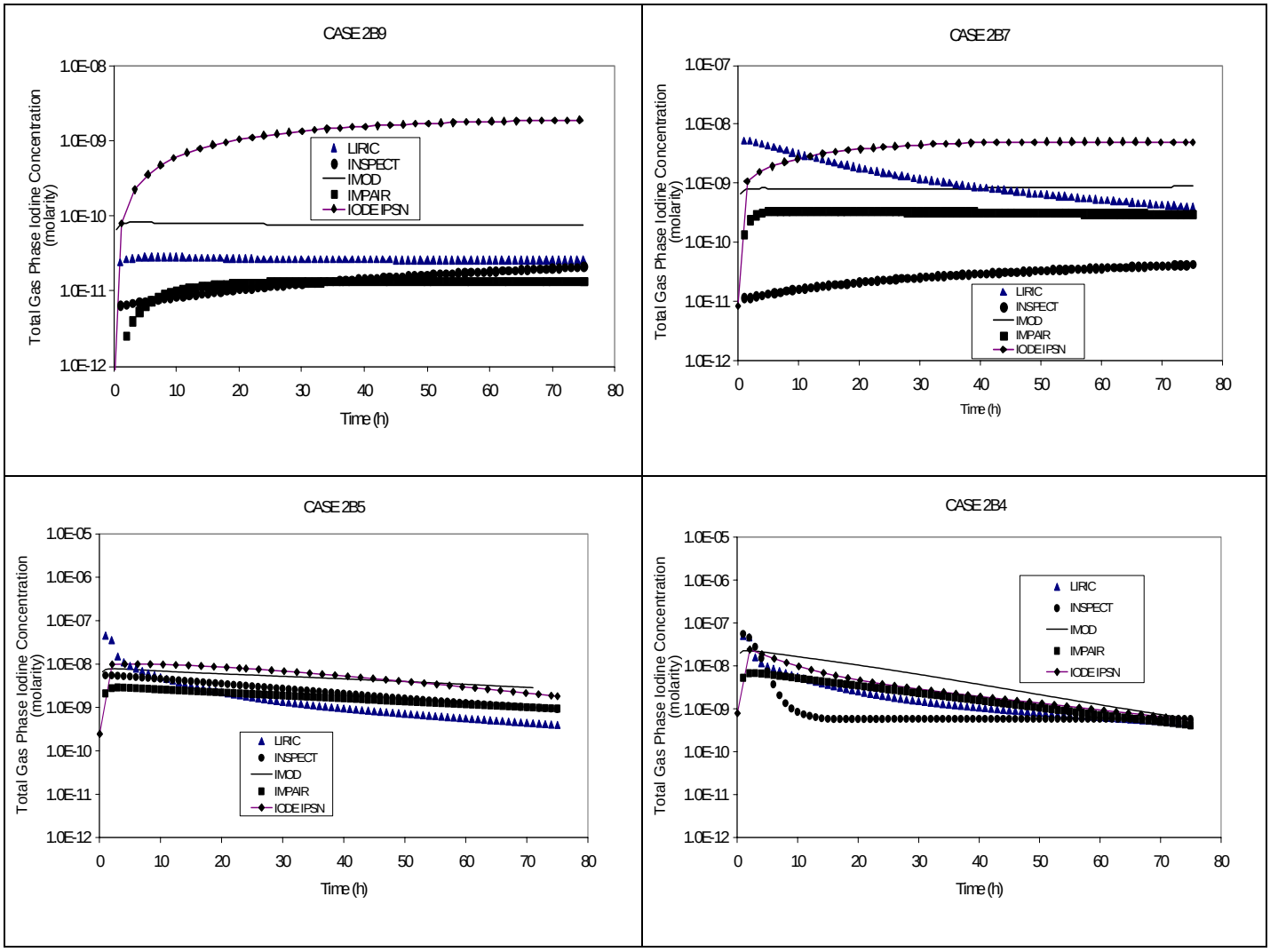

Case 2B. Percentage of iodine inventory in the gas phase for 1×10^{-4} mol·dm^{-3} CsI at 90°C, irradiated at a dose rate of 1 kGy·h^{-1}. No condensation, sump water is assumed to contact painted surfaces.

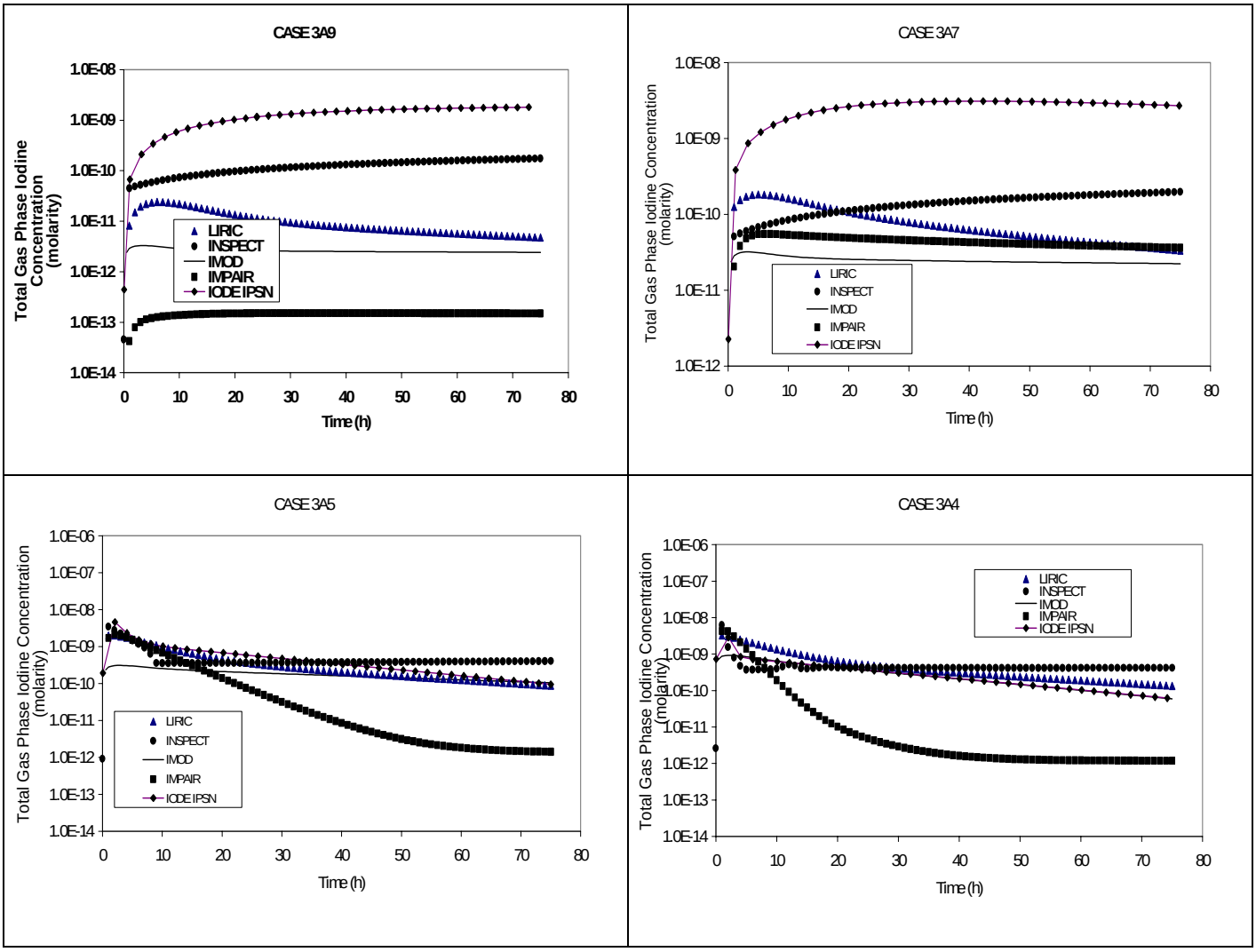

Case 3A. Percentage of iodine inventory in the gas phase for 1×10^{-5} mol·dm^{-3} CsI at 90°C, irradiated at a dose rate of 10 kGy·h^{-1}. No condensation, sump water is assumed to contact painted surfaces.

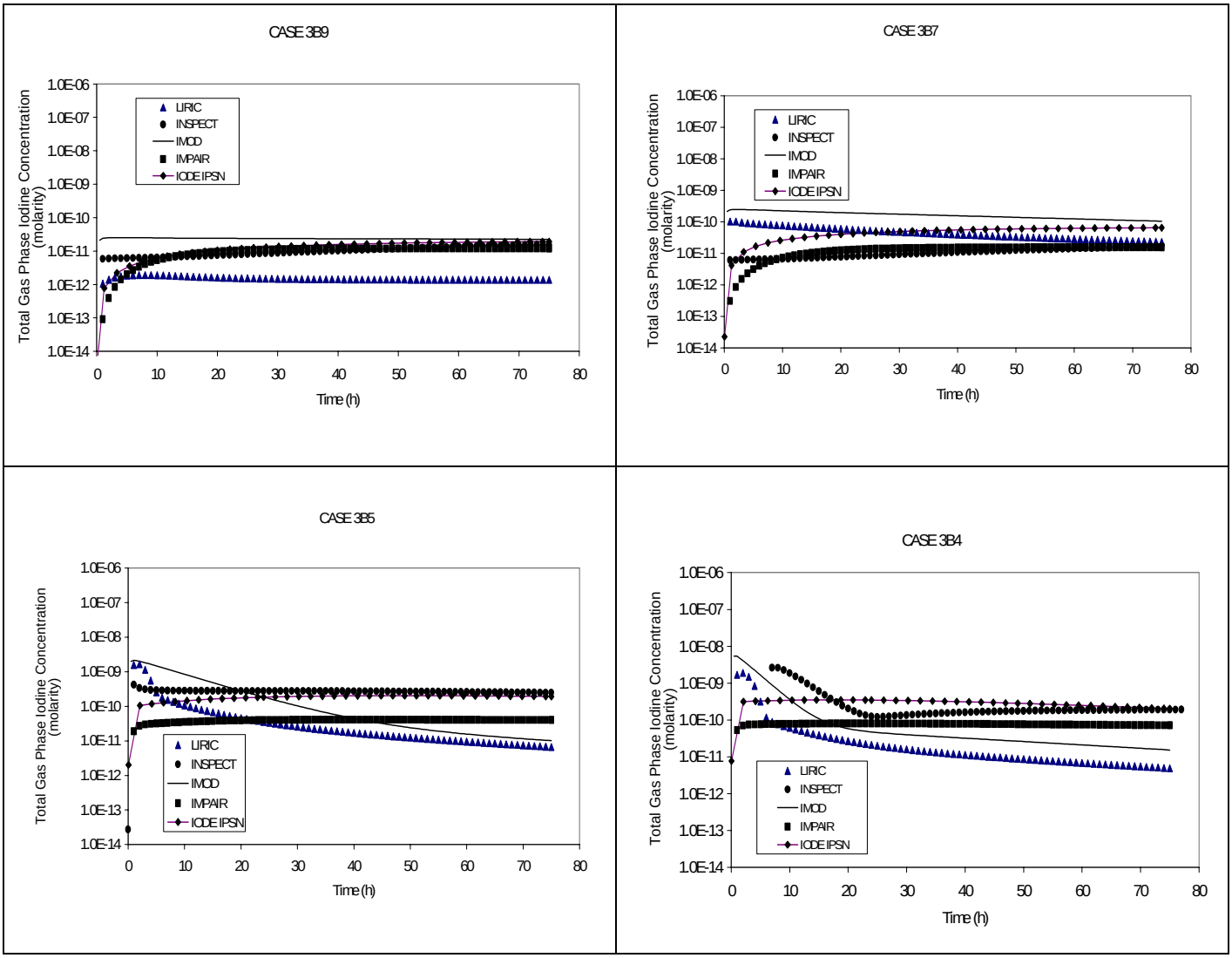

Case 3B. Percentage of iodine inventory in the gas phase for 1×10^{-5} mol·dm^{-3} CsI at 90°C, irradiated at a dose rate of 0.1 kGy·h^{-1}. No condensation, sump water is assumed to contact painted surfaces.

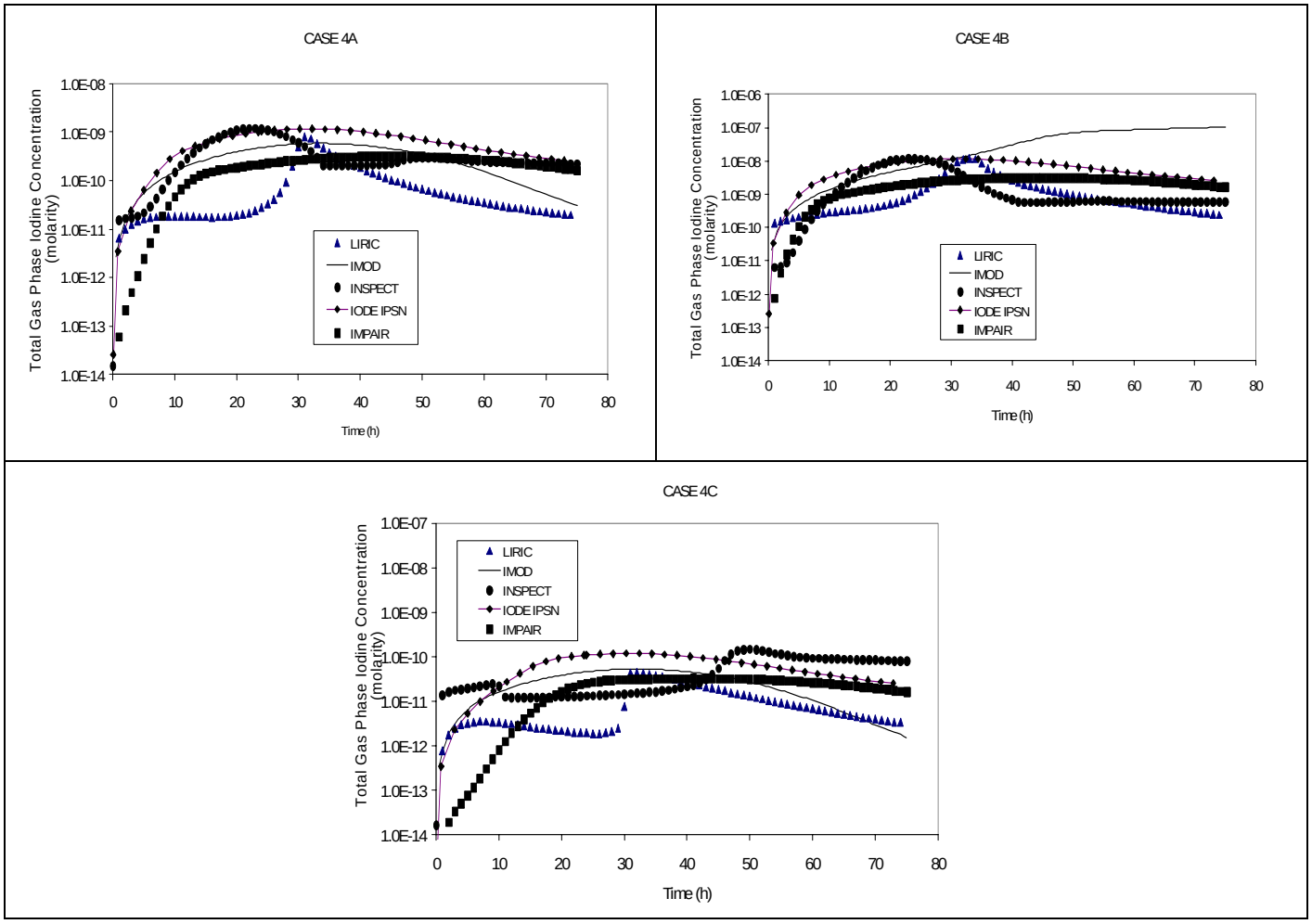

Case 4. Percentage of iodine inventory in the gas phase for (*a*) 1×10^{-5} mol·dm^{-3}, (*b*) 1×10^{-4} mol·dm^{-3}, and (*c*) 1×10^{-6} mol·dm^{-3} CsI at 90°C, irradiated at a dose rate of 1 kGy·h^{-1}. No condensation, sump water is assumed to contact painted surfaces. The pH is assumed to decrease slowly from 10 to 3.5 (see Appendix A).

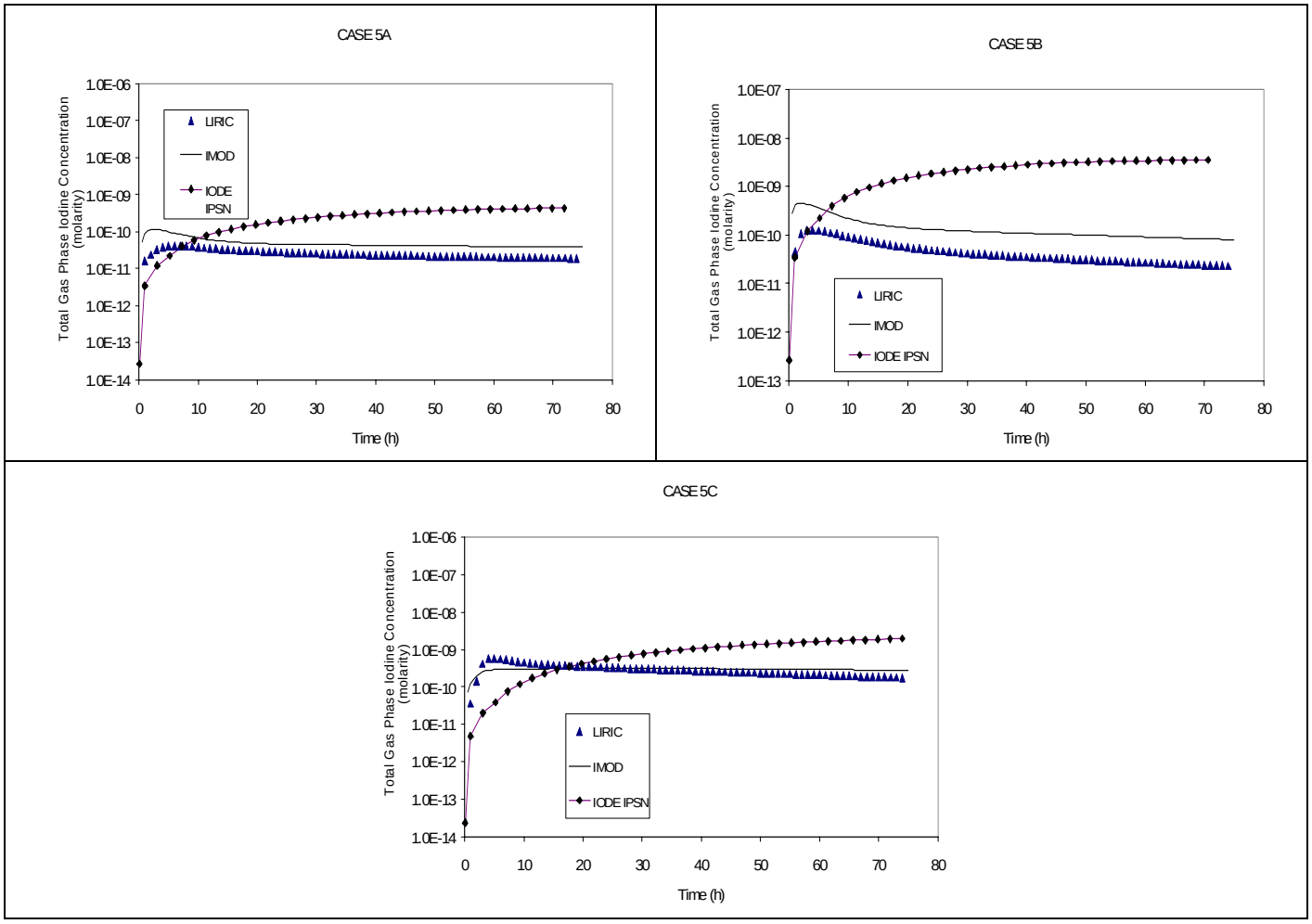

Case 5. Percentage of iodine inventory in the gas phase for 1×10^{-5} mol·dm^{-3} CsI at (*a*) 90°C, irradiated at a dose rate of 1 kGy·h^{-1}; (*b*) 90°C, irradiated at a dose rate of 10 kGy·h^{-1}; and (*c*) 60°C, irradiated at a dose rate of 1 kGy·h^{-1}. No condensation, sump water is assumed to contact painted surfaces.

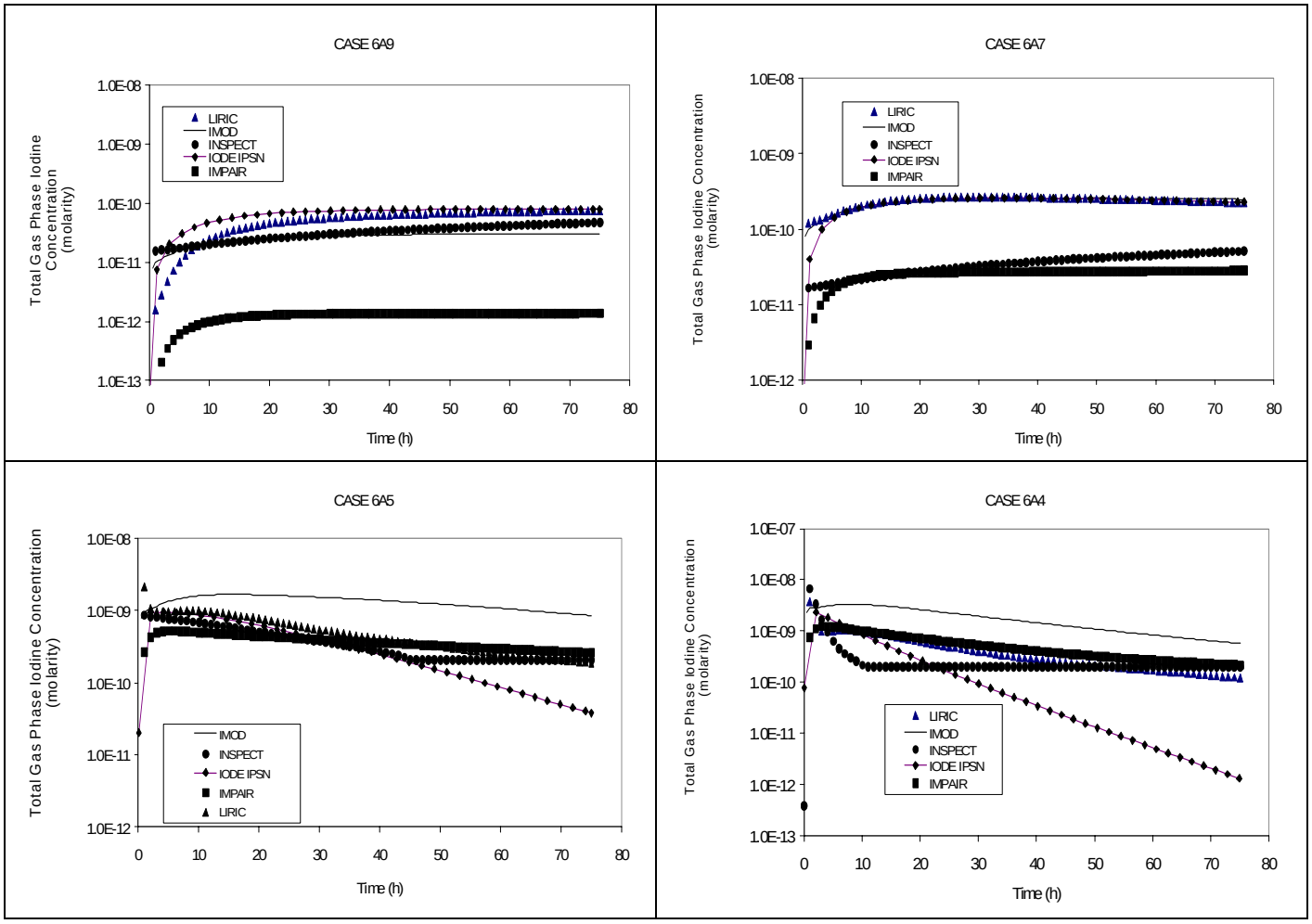

Case 6A. Percentage of iodine inventory in the gas phase for 1×10^{-5} mol·dm^{-3} CsI at 90°C, irradiated at a dose rate of 1 kGy·h^{-1}. Condensing conditions, condensate and sump water are assumed to contact painted surfaces.

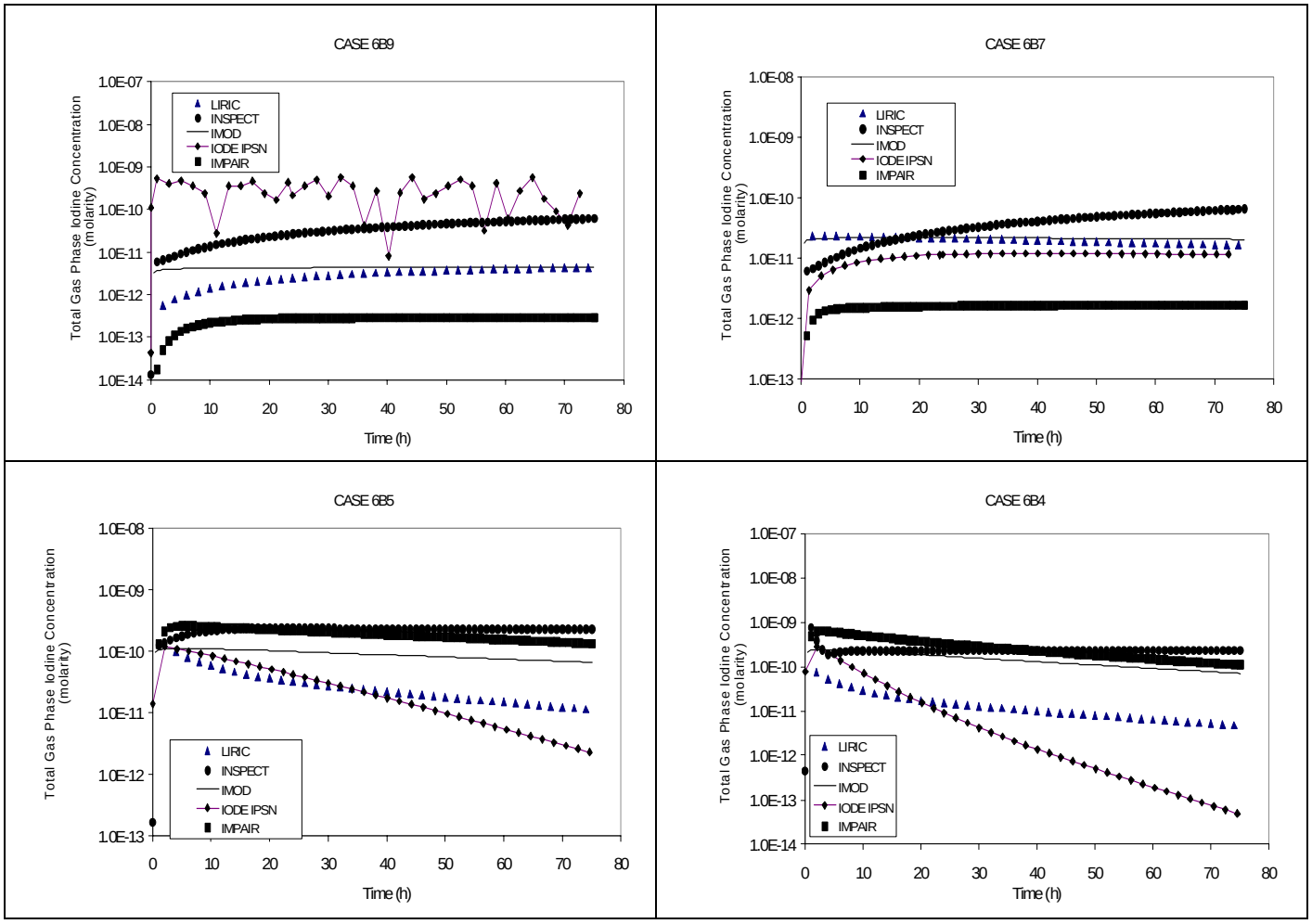

Case 6B. Percentage of iodine inventory in the gas phase for 1×10^{-5} mol·dm^{-3} CsI at 130°C, irradiated at a dose rate of 1 kGy·h^{-1}. Condensing conditions, condensate and sump water are assumed to contact painted surfaces.

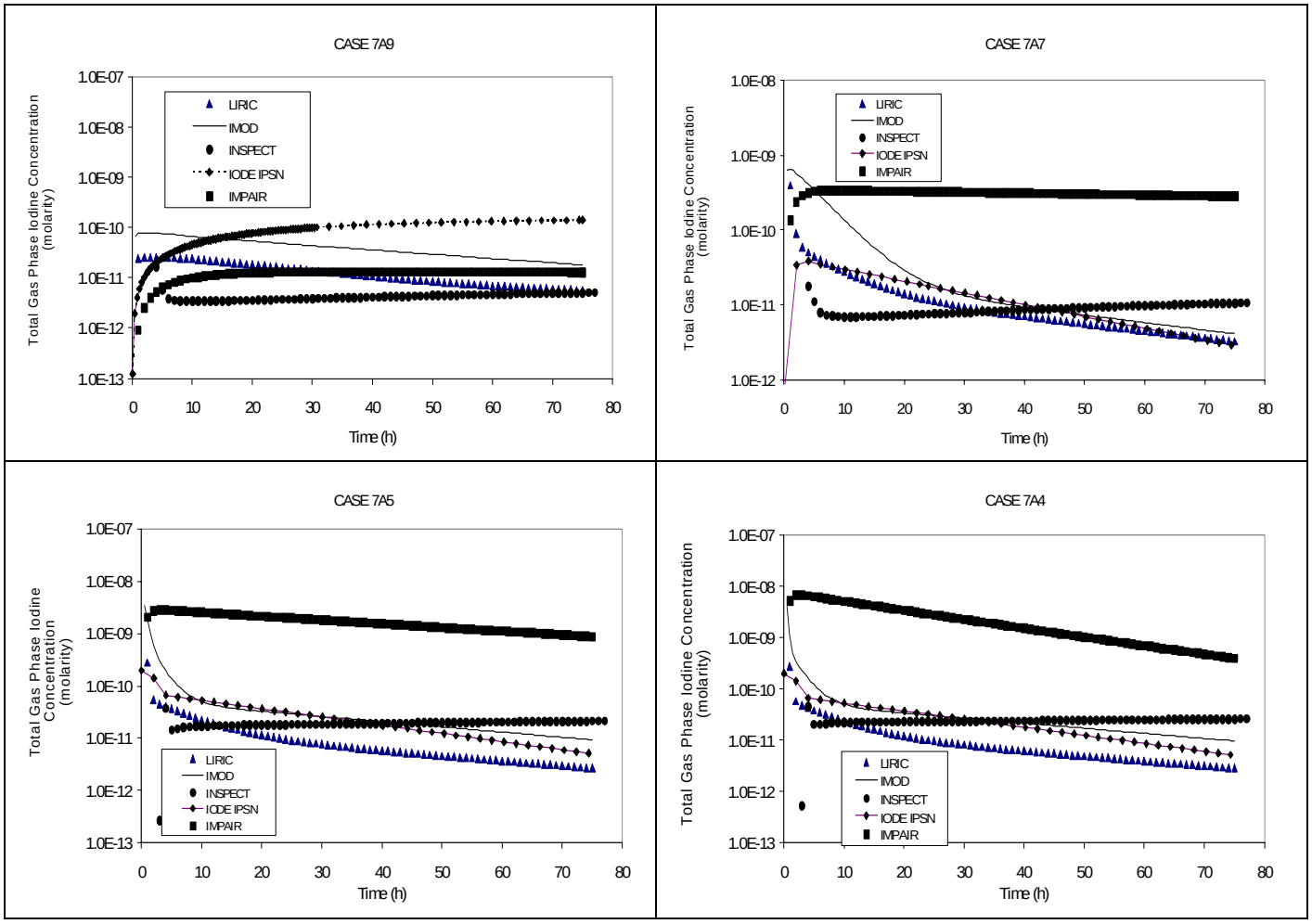

Case 7A. Percentage of iodine inventory in the gas phase for 1×10^{-4} mol·dm^{-3} CsI at 90°C, irradiated at a dose rate of 1 kGy·h^{-1}. No condensation, sump water is assumed to contact painted surfaces. 100 g Ag are assumed to be in the sump water, with 10% of the Ag in the form of AgO.

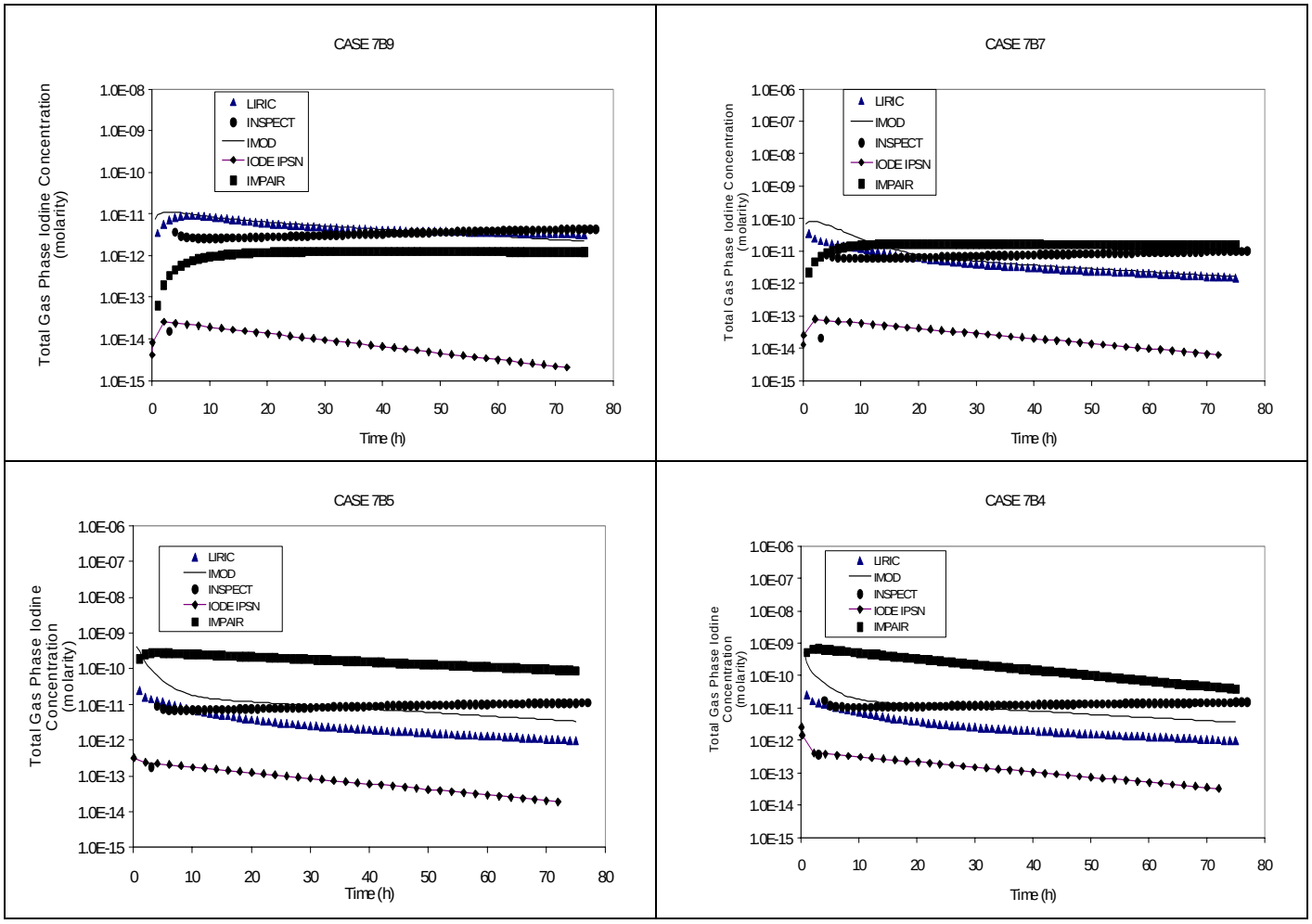

Case 7B. Percentage of iodine inventory in the gas phase for 1×10^{-5} mol·dm^{-3} CsI at 90°C, irradiated at a dose rate of 1 kGy·h^{-1}. No condensation, sump water is assumed to contact painted surfaces. 100 g Ag are assumed to be in the sump water, with 10% of the Ag in the form of AgO.

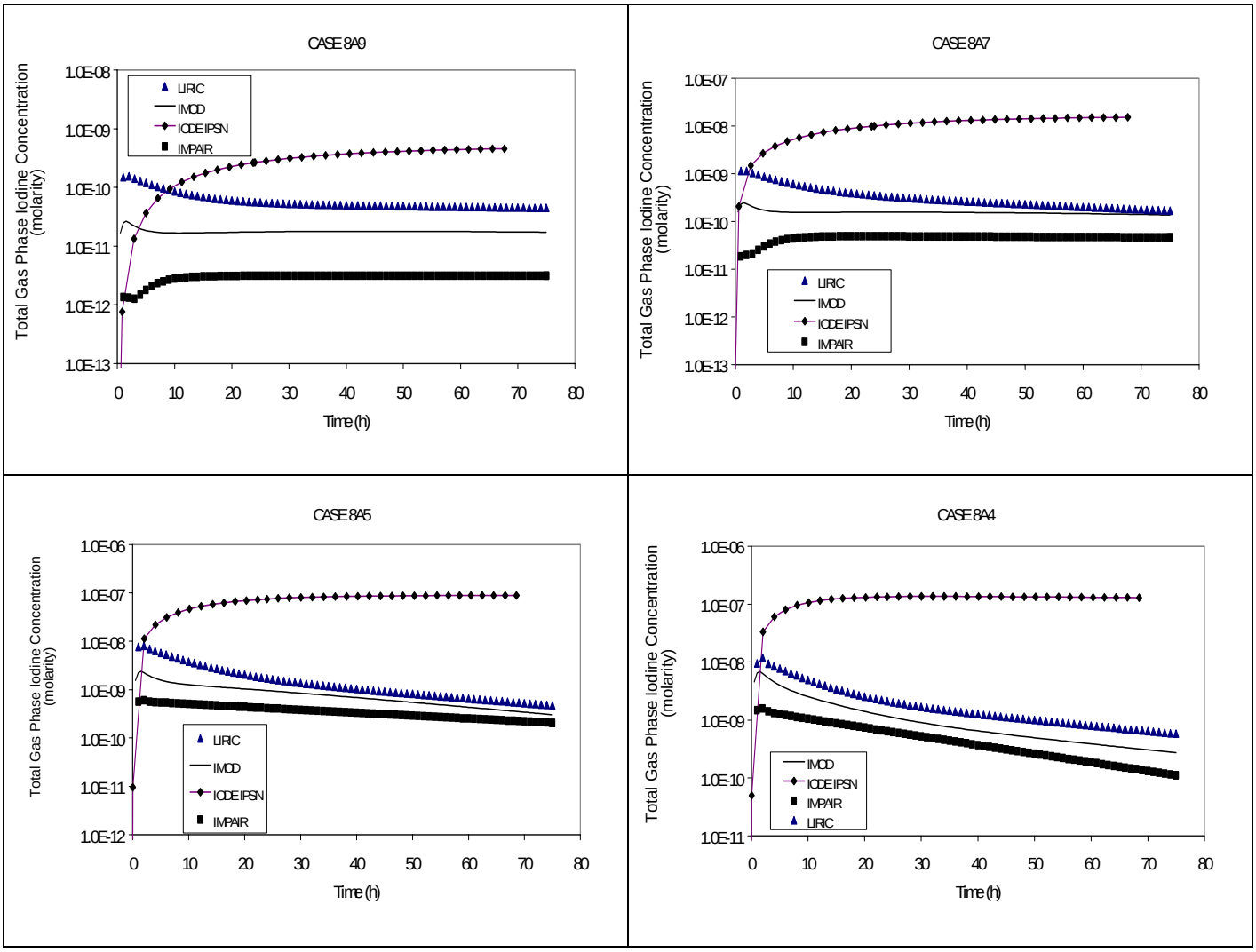

Case 8A. Percentage of iodine inventory in the gas phase for 1×10^{-5} mol·dm^{-3} CsI at 90°C, irradiated at a dose rate of 1 kGy·h^{-1}. No condensation. 1×10^{-3} mol·dm^{-3} organic impurities are assumed to be initially in the sump water.

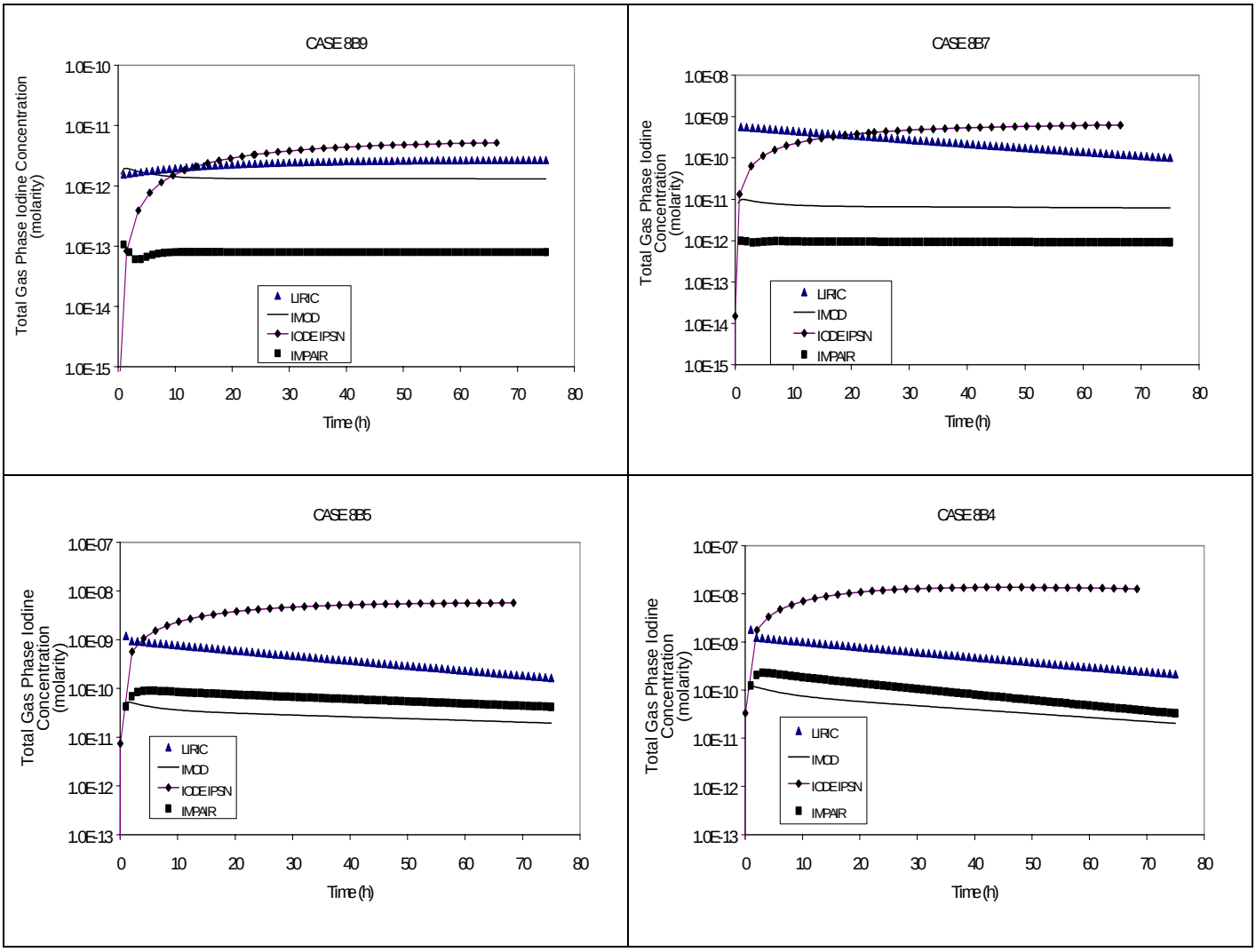

Case 8B. Percentage of iodine inventory in the gas phase for 1×10^{-5} mol·dm^{-3} CsI at 130°C, irradiated at a dose rate of 1 kGy·h^{-1}. No condensation. 1×10^{-3} mol·dm^{-3} organic impurities are assumed to be initially in the sump water.

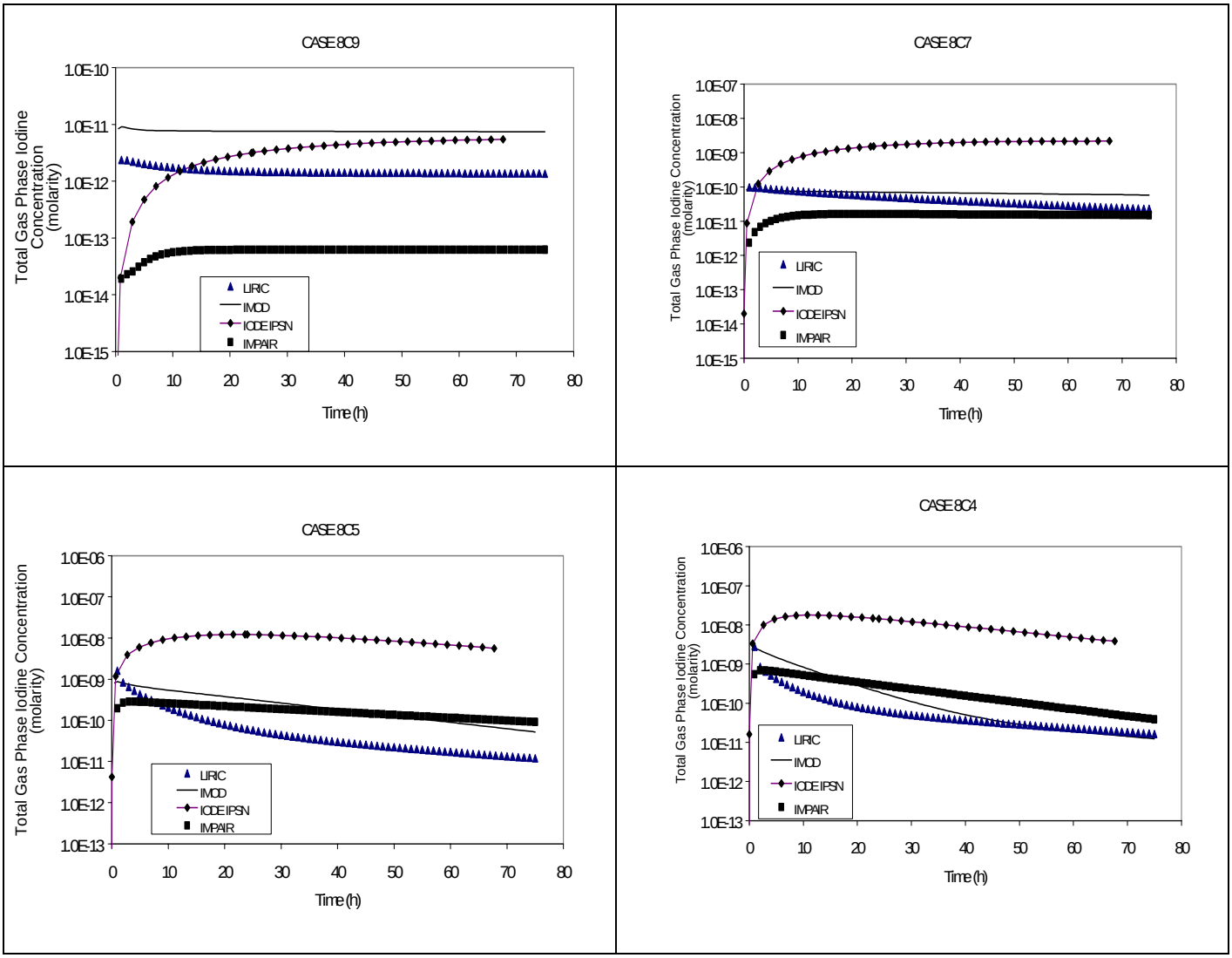

Case 8C. Percentage of iodine inventory in the gas phase for 1×10^{-5} mol·dm^{-3} CsI at 90°C, irradiated at a dose rate of 1 kGy·h^{-1}. No condensation. 1×10^{-5} mol·dm^{-3} organic impurity initially in the sump water.

DISTRIBUTION

W.C.H. Kupferschmidt	10185	CRL 88
D.B. Sanderson	10498	CRL 88
J.M. Ball (5 copies)	10762	CRL 88
L.W. Dickson	05504	CRL 88
R.S. Dickson	20254	CRL 88
S. Sunder	09184	CRL88
M. Stuart	51334	CRL 88
R.J. Lemire	05090	CRL 88
Fuel Safety Branch (2 copies)		CRL 88
M.A. Cormier	08869	SP2F4 - J21
V.G. Snell	03914	SP1F1
R Khaloo	27206	SP2F4
N. Popov	10572	SP2F4 N431
J.N. Barkman	04040	SP4F2
P.J. Allen	06476	SP2F2 N200
M. Bonechi	03136	SP2F1 103
Z. H. Walker	20772	SP2F3 A12
A.G. Lee	10038	SP1F2 E228
G.W. Koroll	05196	WL 34
S.R. Mulpuru	09019	WL 34